NAVAL POSTGRADUATE SCHOOL
Monterey, California

THESIS

A FEASIBILITY STUDY OF LIQUID PHASE SINTER FORMING OF A MODEL CERAMIC SYSTEM

by

Jason Michael Lloyd
September 1998

Co-Advisor: Indranath Dutta
Co-Advisor: Ashok Gopinath

Approved for public release; distribution is unlimited.

DTIC QUALITY INSPECTED 4

19981110 143

REPORT DOCUMENTATION PAGE

Form Approved OMB No. 0704-0188

1. AGENCY USE ONLY *(Leave blank)*	2. REPORT DATE September 1998	3. REPORT TYPE AND DATES COVERED Master's Thesis

4. TITLE AND SUBTITLE A FEASIBILITY STUDY OF LIQUID PHASE SINTER FORMING OF A MODEL CERAMIC SYSTEM	5. FUNDING NUMBERS
6. AUTHOR(S) Jason Michael Lloyd	
7. PERFORMING ORGANIZATION NAME(S) AND ADDRESS(ES) Naval Postgraduate School Monterey CA 93943-5000	8. PERFORMING ORGANIZATION REPORT NUMBER
9. SPONSORING/MONITORING AGENCY NAME(S) AND ADDRESS(ES)	10. SPONSORING/MONITORING AGENCY REPORT NUMBER

11. SUPPLEMENTARY NOTES. The views expressed in this thesis are those of the author and do not reflect the official policy or position of the Department of Defense or the U.S. Government.

12a. DISTRIBUTION/AVAILABILITY STATEMENT Approved for public release; distribution is unlimited.	12b. DISTRIBUTION CODE

13. ABSTRACT *(maximum 200 words)*

The feasibility of a new manufacturing process of ceramic materials in which net shaped products are produced via sintering and simultaneously deforming is studied. A suitable model system of SiO_2-B_2O_3 is chosen due to its desirable properties for liquid phase sintering and its ability to be tested under atmospheric conditions. Samples of compacted powder are prepared and characterized via x-ray diffraction and scanning electron microscopy. Tests to determine the ability of the system to undergo Liquid Phase Sintering are studied. Deformation of samples in compression with concomitant Liquid Phase Sintering at nominally constant true strain rates is performed, and the effects of the amount of liquid phase present are investigated. Problems associated with the Liquid Phase Sinter Forming process are identified, and recommendations are suggested for future studies.

14. SUBJECT TERMS Ceramic Powder Processing, Liquid Phase Sintering, High Temperature Deformation, Superplasticity in Ceramics, Creep Mechanisms, Deformation in the Presence of a Liquid Phase	15. NUMBER OF PAGES 72
	16. PRICE CODE

17. SECURITY CLASSIFICATION OF REPORT Unclassified	18. SECURITY CLASSIFICATION OF THIS PAGE Unclassified	19. SECURITY CLASSIFICATION OF ABSTRACT Unclassified	20. LIMITATION OF ABSTRACT UL

NSN 7540-01-280-5500

Standard Form 298 (Rev. 2-89)
Prescribed by ANSI Std. 239-18 298-102

i

A FEASIBILITY STUDY OF LIQUID PHASE SINTER FORMING OF A MODEL CERAMIC SYSTEM

Jason Michael Lloyd
Lieutenant, United States Navy
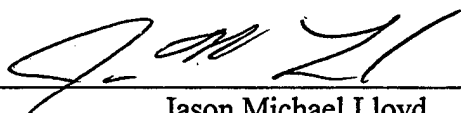B.S. Mechanical Engineering, Florida State University, 1992

Submitted in partial fulfillment of the
requirements for the degree of
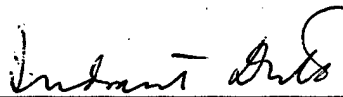
MASTER OF SCIENCE IN MECHANICAL ENGINEERING

from the

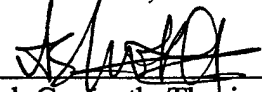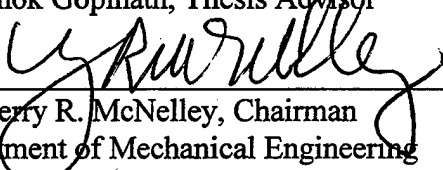## NAVAL POSTGRADUATE SCHOOL
September 1998

Author: _____

Jason Michael Lloyd

Approved by: _____

Indranath Dutta, Thesis Advisor

_____

Ashok Gopinath, Thesis Advisor

_____

Terry R. McNelley, Chairman
Department of Mechanical Engineering

iii

ABSTRACT

The feasibility of a new manufacturing process of ceramic materials in which net shaped products are produced via sintering and simultaneously deforming is studied. A suitable model system of SiO_2-B_2O_3 is chosen due to its desirable properties for liquid phase sintering and its ability to be tested under atmospheric conditions. Samples of compacted powder are prepared and characterized via x-ray diffraction and scanning electron microscopy. Tests to determine the ability of the system to undergo Liquid Phase Sintering are studied. Deformation of samples in compression with concomitant Liquid Phase Sintering at nominally constant true strain rates is performed, and the effects of the amount of liquid phase present are investigated. Problems associated with the Liquid Phase Sinter Forming process are identified, and recommendations are suggested for future studies.

TABLE OF CONTENTS

I. INTRODUCTION

Ceramic materials are inorganic, either ionically or covalently bonded compounds between metallic and nonmetallic elements. Primitive civilizations determined that when water was added to clay minerals, the resulting solution became plastic and easily molded into desired shapes. The shape could be dried in the sun and hardened in a high temperature fire to produce what are known as the traditional ceramics such as pottery, china and bricks [Ref. 1]. Within the last half century, a revolution in materials engineering has led to a new generation of ceramics that require tightly controlled microstructure, chemical composition and processing. Phenomenal progress has been made in understanding the fundamental characteristics of these materials, and how to capitalize upon their desirable mechanical, thermal and electrical properties.

The ceramic industry is one of the largest in the United States, and is developing rapidly. The industry is unique in that it is essential for the successful operation of numerous different manufacturing enterprises. Uranium oxide fuels, for example, are essential to the nuclear-power industry while glass products are crucial to the construction and automotive industries. The future potential applications of ceramic materials are innumerable, and the bounds of their use continue to grow as we learn more about harnessing their desirable properties.

Some of the familiar characteristics of ceramics are that they are extremely strong and brittle, fracturing with little or no plastic deformation. These unique properties stand in stark contrast to those of metals, which yield and plastically deform under an applied stress. Ceramics, therefore, cannot be processed into desired shapes using the familiar metallic deformation processes. In the post World War II era, extensive efforts were

made throughout the western world to fabricate ceramics under high temperature operations utilizing conventional metallurgical processing such as extrusion, rolling and forging. The goal was to produce ceramic parts during the actual ceramic production in order to avoid the expensive machining processes required by ceramics. The work led to an improved understanding of ceramic deformation processes, but the requirement for extremely high forming temperatures forced the concept of thermomechanical processing of ceramics to be abandoned [Ref. 2].

Conventional processing of ceramics involves many steps [Refs. 3-5]. Ceramic particles are first crushed in a milling process to produce very fine powders. The ground powder is mixed with a number of additives such as binders, lubricants, plasticizers and deflocculents in order to impart desirable properties to the mix. The mixture is molded into a desired shape in one of two basic shaping processes. In *slip casting*, the mixture is added to a liquid such as water resulting in a suspension of ceramic particles in the liquid (slip). The slip is poured into a plaster mold of the desired shape. The porous mold absorbs some of the water from the suspension and the soft solid of the desired shape is removed from the cast. In the second shaping process, called *pressing*, the powder mixture is placed into a compact and bonded via pressure. Heating the compact while it is being pressed can enhance the solidification process, and uniform properties can be achieved by isostatic pressing. The resulting product from either shaping process is a weakly bonded solid with very low "green" strength. In order to gain the desirable properties, the shaped product must be dried and fired or *sintered*. In the sintering process, the part is heated to an elevated temperature in a controlled environment to densify the product. As a result of the reduced porosity, some shrinkage of the part

2

occurs during the firing process. The resulting ceramic is then shaped into a final product via post-fire machining. Elimination of the post-fire machining step would be a monumental breakthrough, since this step is expensive and can account for 90% of the cost of a finished part [Ref. 6].

The process of sintering can be accomplished via either a solid state process or a process known as liquid phase sintering. The first process relies on solid state diffusion between adjacent particles in order to achieve densification. In order to achieve satisfactory solid state sintering, the sintering temperature must be about 80% of the melting temperature of the solid. Since the melting temperature of most ceramics is extremely high, solid state sintering is difficult to achieve for these materials. In liquid phase sintering (LPS), a low melting point additive, known as a sintering aid, is combined with the powder to be sintered. This additive provides a liquid phase at a relatively low temperature that provides a short circuit path of diffusion, resulting in enhanced sintering rates [Ref. 3]. This thesis pertains to the later phenomenon (LPS).

The advantages of creep deformation of materials with a small amount of liquid phase present at the grain boundaries have been recognized, and utilized for years. Construction workers take advantage of the deformability of concrete containing liquid in order to shape into a desired final product prior to solidification, and dentists utilize the fact that amalgam contains a small amount of liquid to allow deformation of fillings prior to setting in a cavity. The question under consideration is whether or not a ceramic product can be manufactured in a simpler method. Can the powders comprising a ceramic be sintered with a small amount of liquid phase present and *simultaneously* deformed to achieve the desired final shape? The advantages of a process such as this

3

are substantial, as it would eliminate the often cost-prohibitive post-fire machining process. The objective of this endeavor is to study the combined phenomena of liquid phase sintering (**LPS**) with concomitant deformation in order to investigate a unique approach for production of ceramic products.

II. BACKGROUND

A.   PROCESSING CERAMIC POWDERS

Ceramic production usually starts with a fine powder, which permits the fabrication of complex shapes due to its packing properties. The processing of ceramic powders into a solid compact with a green strength generally takes place in four stages: powder selection, processing, preconsolidation and consolidation.

1.   Powder Selection

The desired properties of the end product ultimately determine the ceramic powder selected for processing. When selecting a powder for a specific application, one must consider purity, particle size distribution and reactivity [Ref. 4].

a.   *Purity*

Impurities can have detrimental or beneficial effects on high temperature properties such as strength, rupture life and oxidation resistance. Impurities present as inclusions can cause local stress concentrations and decrease the component tensile strength, but do not adversely affect creep or oxidation of the material [Ref. 5]. Impurities can also have an advantageous effect on the superplastic properties of a ceramic if the impurity is one that can form a grain boundary glassy phase at a relatively low temperature [Ref. 7]. This phenomenon is due to enhanced grain boundary sliding in the presence of a liquid phase.

b.   *Particle Size and Reactivity*

Particle size distribution is important to ensure the efficient packing of the ceramic powders. Maximum particle packing decreases porosity and, thus, minimizes

shrinkage during the densification phase. Employing a single particle size can result in over 30 % porosity; to achieve optimum packing, a range of particle sizes is required [Ref. 5]. The driving force for densification of a ceramic powder is the change in its surface free energy. Small particles have a large surface area to volume ratio and thus have a strong thermodynamic driving force to reduce their surface free energy by coalescing with adjacent particles. Typically, the temperature and time at temperature required for complete densification decrease as particle size is reduced [Ref. 3]. Additionally, smaller particle sizes yield finer grain sizes in the final product. The goal, therefore, must be to minimize the mean particle size while subsequently ensuring an adequate range of sizes for processing.

2. Powder Processing

When a powder is purchased for a particular application, the particle size is generally not as fine as would be desired for optimal performance. As mentioned previously, the control of particle size and size distribution has a strong effect on the porosity of the powder compact and its resulting mechanical properties. The powder processing stage is used to achieve this optimum size distribution via either a mechanical or chemical means.

a. *Mechanical Sizing*

There are numerous mechanical sizing methods to process powders such as fluid energy milling, hammer milling, and vibratory milling [Ref. 8]. One of the most common types of mechanical sizing is a process known as ball milling. In ball milling, the powder to be milled, which is called the *charge*, is placed in a cylinder along with a grinding medium in the shape of balls, rods or small cylinders. The cylinder is rotated

axially, allowing the media to cascade and mill the powder. Milling can be performed either wet or dry. In wet milling, the charge is mixed with a liquid of low vapor pressure in the mill before the rotation stage. Wet milling results in a finer particle size and a narrower size distribution [Ref. 8]. After milling, the slurry is heated so that the liquid boils off and leaves a fine powder residue. Dry milling avoids the problems associated with boiling the liquid off after sizing, but has the major disadvantage that powder tends to pack into the corners of the mill and avoid the grinding media. This problem can be minimized by mixing in about 0.5 weight percent of a lubricant such as zinc stearate or polyethylene glycol to minimize particle friction and affinity for moisture. The lubricant thus preventes agglomeration of the powder in the mill corners [Ref. 5].

b.   *Chemical Sizing*

Chemical sizing has the advantage of minimal particle contamination and tight control over particle size distribution. Some common types of chemical sizing are precipitation, freeze-drying and spray roasting [Ref. 8].

c.   *Size Determination*

Screening is the primary means of particle sizing. During the screening process, the powder is poured onto a sieve having a selected size opening. By utilizing sieves with different size openings, the particle sizes can be separated into ranges. Screen sizes are classified according to the number of openings per linear inch, and are referred to as mesh sizes [Ref. 5]. A 300-mesh screen, for example, has 300 equally spaced openings per linear inch.

7

3.   Preconsolidation

Once the powder has been selected, processed and sized, it is ready for the preconsolidation stage. During this stage, the sized powders are mixed with several additives in preparation for the consolidation stage. To achieve a final component having uniform properties and no distortion, several additives must be mixed with the powder. Some common additives are binders, lubricants and sintering aids.

a.   *Binders*

Binders are added to provide strength in the "green," or unfired compact. The binder acts as a type of glue between the particles in the compact. The addition of a binder is critical in order to permit handling prior to the densification stage. Some common binders are polyvinyl alcohol (PVA), waxes, thermoplastic and thermosetting resins [Ref. 5].

b.   *Lubricants*

The purpose of the lubricant is to allow particles to slide over one another during the compaction process. Particle to particle and particle to die-wall friction must be reduced during the compaction process so that the powder particles can slide over one another in order to pack efficiently and eliminate porosity.

c.   *Sintering Aids*

Sintering aids are also used to aid in densification. The addition a small amount of a low melting point ceramic that can form a glassy phase at the grain boundaries during sintering will enhance grain boundary sliding and permit reduced porosity and a shorter sintering time [Ref. 3].
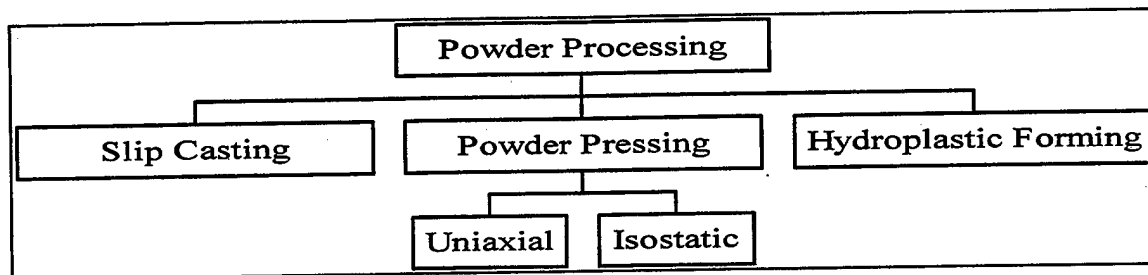
Figure 1. Schematic of the powder compaction processes available for densification of ceramic powders.

4.   Powder Consolidation

After the additives and powder have been thoroughly mixed in a ball mill, the solution is ready for consolidation. The powder solutions are formulated into their desired shape by hydroplastic forming, powder pressing or slip casting (Figure 1).

Uniaxial powder pressing is the most common method of powder consolidation for high volume productions [Ref. 6]. The compaction pressure results in compact densification via particle rearrangement and deformation. The porosity and volume of the compact decrease as the pressure increases, while the coordination number of the particles, green density and compact strength all increase. The objective of the pressing process is to form a relatively defect free, uniformly dense, net shaped powder compact. To achieve this goal, one must first understand the causes of compact defects and then minimize defects by countering the causes. Frictional effects and springback are the major causes for various types of compact defects.

Frictional losses between particles and the die wall decrease the compaction pressure available as the distance into the compact increases. A uniaxial pressure that is applied to a powder compact is thus dissipated via frictional forces. As a result, some portions of the compact will experience much lower than the applied pressure. Since the density of packing is directly proportional to the applied pressure, density gradients exist within the compact. These density gradients can result in warpage, distortion or cracking

9
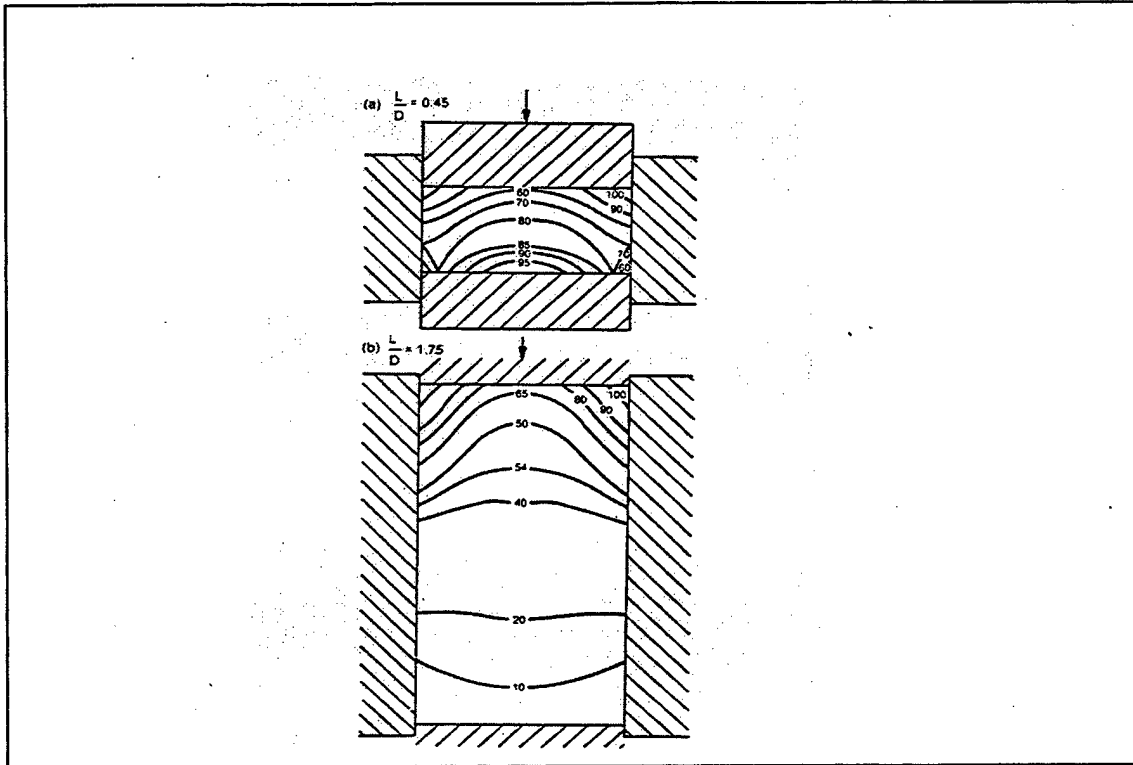
Figure 2. Schematic showing density variations in typical powder compacts due to particle-particle and particle-die wall friction. (From Ref. 5)

during the sintering process [Ref. 5]. As seen in Figure 2, the density variations increase

as the aspect ratio increases due to the larger pressure gradients. Using lubricants on the

die walls and punches, isostatic pressing or low aspect ratio compacts will minimize

losses due to die wall friction [Ref. 6]. Several recent studies have revealed that density

gradients exist in compacts that have been isostatically pressed so that no wall frictional

forces are present [Ref. 9]. These findings indicate that inter-particle frictional forces can

also affect compact density. Using a lubricant in the powder processing stage minimizes

the inter-particle frictional forces.

Springback is defined as the expansion of the compact upon ejection from the die

in a direction perpendicular to the pressing direction. This phenomenon occurs as a result

of the residual stresses in the compact after ejection from the dye. Differential
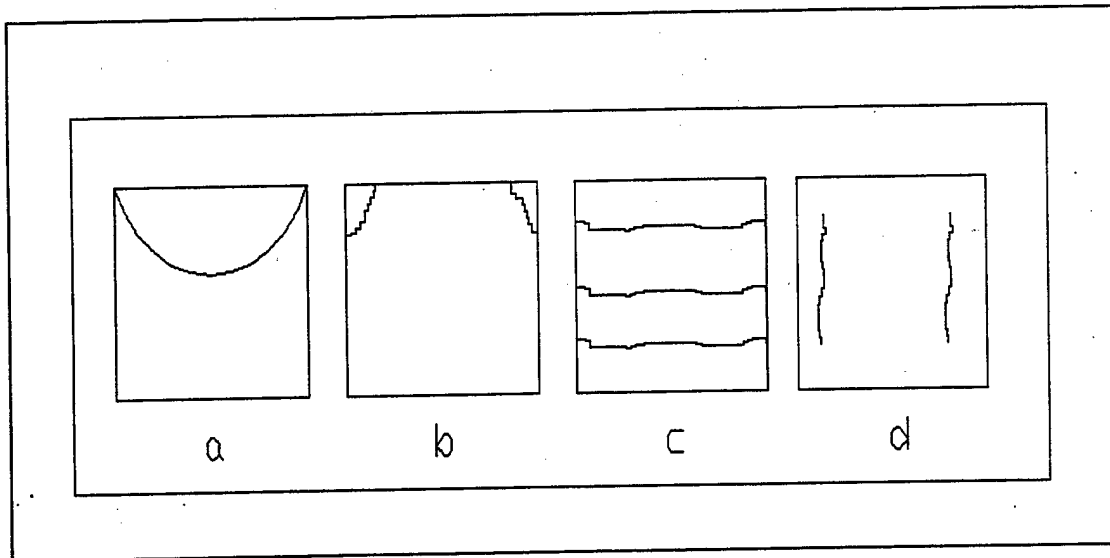
Figure 3. Schematics showing (a) end capping, (b) ring capping, (c) laminations and (d) vertical crack defects. (After Ref. 6)

springback is springback in the direction parallel to the direction of compaction. Excessive springback will produce catastrophic flaws in the compact. Limiting the compaction ratio below a threshold value minimizes effects of springback [Ref. 6].

Frictional effects and springback lead to various types of compaction defects. Some common compaction defects are: end capping, ring capping, laminations and vertical cracks (Fig. 3).

a. *End Capping*

After a compact has been compressed and the pressure is released from the punch, the material rebounds near the top center of the compact. Frictional forces on the die walls prevent the powder compact near the walls from rebounding. A tensile stress thus exists near the upper edges of the compact, and cracking may result. A cone shaped separation near the face of the pressing punch is evidence of end capping. Minimizing die wall frictional forces minimizes end capping effects [Ref. 5].

11

b. *Ring Capping*

A separation around the outer edge of the pressing punch face is evidence of a defect known as ring capping. These defects are caused by poor machining tolerances between the punch and the die, and are minimized by improving these tolerances.

c. *Laminations*

When a compact is being ejected from a die, as part of the compact clears the top of the die, the material will rebound to a larger cross section in order to reduce residual stresses. This places a tensile stress in the material just above the top of the die and can result in a repeating series of circumferential cracks. These repeating circumferential cracks in a compact indicate defects known as laminations. These defects occur when particle-particle friction effects are high and large aspect ratio compacts are made.

d. *Vertical Cracks*

Cracks that form parallel to the pressing direction are evidence of vertical cracks that are the result of differential springback. These defects are problematic in compaction processes with high aspect ratios.

Once the compact has been compressed, it is called a *green compact* and has *green properties*. These properties are often measured in order to determine if the compact has any flaws and to predict the properties of the final sintered product utilizing previously derived correlations [Ref. 10]. The bulk density of simple shapes is usually determined by weighing the compact and measuring the dimensions. The density of
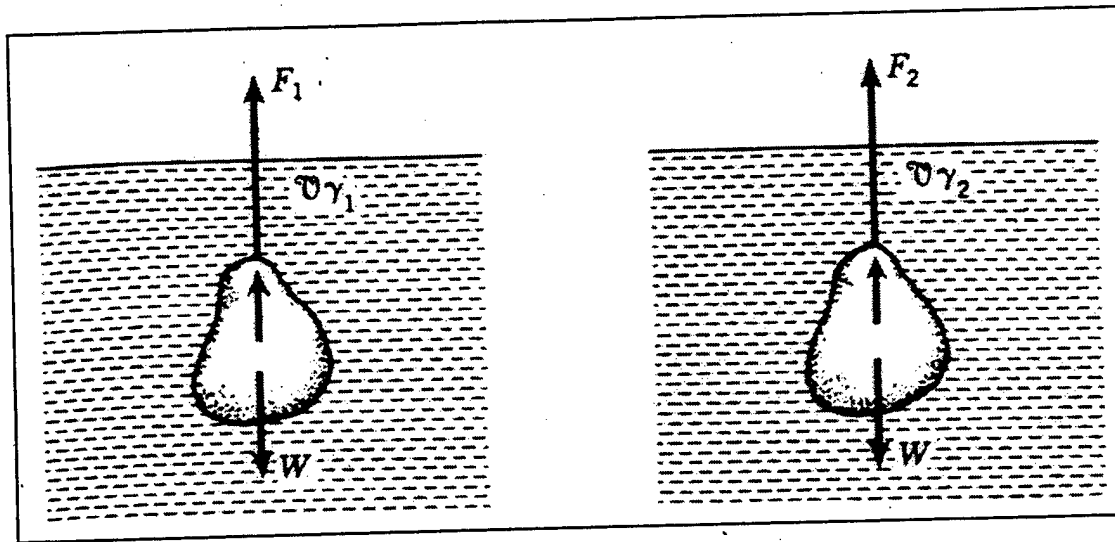
Figure 4. Free-body diagrams of a weight suspended in fluids of different specific gravity. (From Ref. 27)

complex shapes is determined using the immersion-density technique (i.e., Archimedes' method) [Ref. 10].

Determining the density of an object utilizing Archimedes' method is a simple application of the laws of buoyancy (Fig. 4). The body is first suspended in a liquid of specific gravity γ_1 and the force F_1 is measured and recorded. The object is then immersed in a fluid of specific gravity γ_2 and the force F_2 is measured. The equations of static equilibrium are thus given by:

$$F_1 + V\gamma_1 = W \qquad\qquad F_2 + V\gamma_2 = W \tag{1}$$

Solving these equations simultaneously for the Volume V and weight W:

$$W = \frac{F_1\gamma_1 - F_2\gamma_2}{\gamma_2 - \gamma_1} \qquad\qquad V = \frac{F_1 - F_2}{\gamma_2 - \gamma_1} \tag{2}$$

13

The density of the compact is then calculated directly as $\rho = W/gV$. The fact that most green compacts have surface porosity dictates that the compact be coated with a wax prior to density determination via Archimedes' method [Ref. 10].

B.   LIQUID PHASE SINTERING

Sintering is a process in which previously compacted powders are heated to a temperature below their melting temperature in a controlled atmosphere in order to facilitate bonding between the particles. In the event that one of the constituents of a system melts and forms a solid/liquid interface with the other constituents, the sintering process is referred to as liquid phase sintering (LPS). The presence of a liquid phase during the sintering process usually increases the rate of sintering [Ref. 4]. Many products today are formed via the process of LPS, including automotive connecting rods, small gears, wristwatch components, and refractory ceramics.

There are two basic types of liquid phase sintering [Refs. 3-5]. In type 1 LPS, the liquid is present throughout the duration of sintering between the solidus and liquidus components. In the type 2 LPS, sometimes termed "transient liquid phase sintering," the liquid forms when the compact is heated to the sintering temperature, but is either carried away through evaporation or disappears via diffusion into the solid while the compact is at the sintering temperature. The densification and growth process of the type 1 LPS described above can be analyzed in three stages [Refs. 3-4].

1.   Rearrangement

During heating of the compact, solid-state sintering occurs between the particles primarily due to the chemical concentration gradient in the microstructure [Ref. 3]. Once

14

the eutectic temperature of the system is reached, liquid of eutectic composition melts, and there is an accompanying rapid increase in the densification rate due to particle rearrangement. The amount of densification that can be achieved via rearrangement is proportional to the amount of liquid present. A high percentage of liquid at the grain boundaries results in nearly full densification during this stage, while a low percentage of liquid results in a solid skeleton which restrains densification. Capillary action allows the liquid phase to infiltrate the interstices; the small capillaries getting filled first and the larger capillaries next, depending upon the availability of liquid. Simultaneously, the solid particles themselves rotate and rearrange so as to fill space as efficiently as possible. At the end of this stage, however, significant porosity is still present, usually associated with the larger interstitial spaces between particles. The elimination of porosity results in a continual increase in the compact's viscosity causing the densification rate to continually decrease during this stage [Ref. 3].

2. Intermediate or Solution Reprecipitation Stage

When further densification is no longer feasible via rearrangement of particles and flow of the liquid phase into the interstices, solubility and diffusivity effects become significant. Continued densification and grain growth occurs by the process of dissolution of the solid phase in the liquid and re-precipitation upon existing grains.

The extent to which a compact can densify via this stage of **LPS** is strongly dependent upon the extent of solid solubility in the liquid phase. As the number of pores in the compact decreases, *grain shape accommodation* must occur in order to lower the surface free energy associated with the system (Fig. 5). During the solution–reprecipitation process, the growing solid grains change their shape from spherical to

15
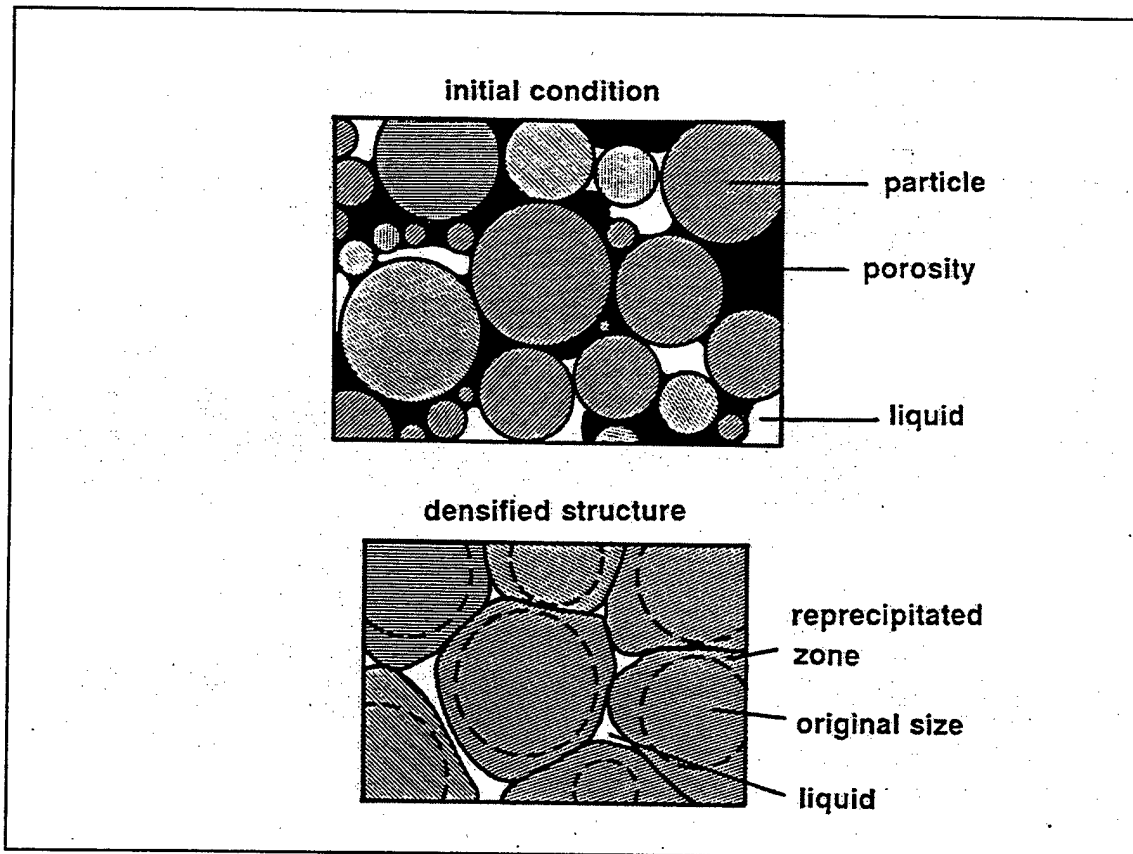
Figure 5. Diagram showing the elimination of pores by grain shape accommodation solution-reprecipitation. (From Ref. 3)

effectively eliminate space [Ref. 3]. Since the new grain shape has a higher solid-liquid surface area than a sphere with the same volume, an increase in the system free energy occurs. This increase is offset, however, by elimination of the pores and their associated free surface energy [Ref. 3]. Grain shape accommodation can take place via one of three mechanisms (Fig. 6).

In the first mechanism, known as contact flattening, capillary forces from the liquid induce a stress at the point of grain contact. In order to relieve the stress, some solid dissolves into the liquid at the contact point, and redeposits on areas away from the contact point. Grain shape accommodation occurs due to the center-to-center motion of neighboring grains. It should be noted that smaller grains would increase the effective
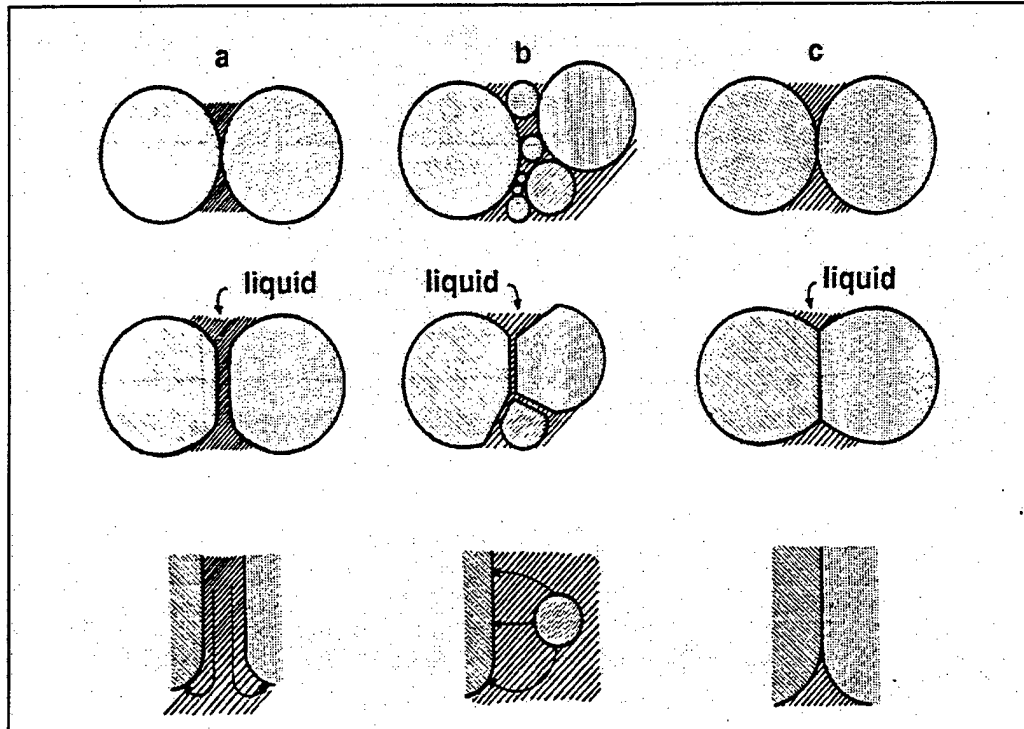
Figure 6. Diagram showing the possible grain shape accommodation mechanisms during liquid phase sintering. The possible mechanisms are (a) contact flattening, (b) dissolution of fine grains, and (c) solid-state diffusion. (From Ref. 3)

capillary stress and result in higher rates of contact flattening. For a given capillary

force, as the size of the area of contact grows, the stress induced in the contact region

diminishes ($\sigma=F/A$). The rate of dissolution will thus decrease and the rate of

densification will slow.

The second mechanism of grain shape accommodation relies on solid particles of

a range of sizes. In this circumstance, the smaller particles have a large free energy

associated with their high surface area to volume ratio, and are thus more likely to

dissolve into the liquid phase to minimize this free energy than the larger particles. The

difference in solubilities results in a concentration gradient in the liquid. The smaller

particles thus dissolve in the adjoining fluid, are transported to, and re-precipitate on one

of the larger solid grains. This process is often referred to as *Ostwald ripening* [Ref. 3].

The net result is the growth of larger grains at the expense of the smaller ones. Since the small grains redeposit only on specific areas of the larger grains, grain shape accommodation takes place with a decreasing pore volume.

The third mechanism of grain shape accommodation relies upon contact flattening, but the mechanism is solid state diffusion. Due to the fact that the rate of diffusion through the liquid is usually much higher than the rate of solid-state diffusion, this mechanism is usually considered negligible during the intermediate densification stage.

It is interesting to note that while grain growth is inextricably linked with the dissolution and reprecipitation mechanism, contact flattening involves no grain growth. Experimental observations of liquid phase sintered compacts show grain growth and thus support the solution-reprecipitation mechanism [Ref. 3]. Due to the fact that initial contact stresses are extremely large as a result of point contact between two spherical particles, it is intuitively obvious that contact flattening is initially important in the intermediate stage. As the rate of densification via contact flattening decreases as a result of increased contact surface area, the mechanism of dissolution and reprecipitation of small grains will begin to dominate the process [Ref. 3].

If the liquid phase has a relatively high viscosity, as in the case of ceramics with a glassy grain boundary phase, the viscosity can inhibit the forces necessary to cause contact flattening. Further raising the sintering temperature in order to reduce the viscosity can minimize this factor [Ref. 3].

3.   Solid State Sintering

In many cases of liquid phase sintering, complete densification is achieved during stages one and two. Holding the compound at the sintering temperature for a prolonged period may lead to immoderate grain growth and general degeneration in compact material properties [Ref. 4]. In the case where a long-range skeletal system of solid phase forms prior to complete densification, further densification can only be realized via solid-state sintering [Ref. 3]. Densification during this stage is extremely slow as compared to rates in the first two stages due to the rigid skeleton of contacting grains. This mechanism is active throughout the sintering process, but is not significant until after stages one and two have occurred.

In transient liquid phase sintering, a fourth stage exists in which the compact is held at the sintering temperature in order to allow the liquid to evaporate or diffuse [Ref. 4]. This phase is carried out in order to minimize possible detrimental effects of having residual liquid (the low melting phase) present at the grain boundaries in the final microstructure.

C.   HIGH TEMPERATURE DEFORMATION

Creep deformation is defined as the time-dependent and permanent deformation of a material when subjected to a constant load or stress [Ref. 1]. It is generally observed in both crystalline and non-crystalline materials. Creep deformation can be divided into two major categories depending upon the mechanism: dislocation creep or diffusional creep.
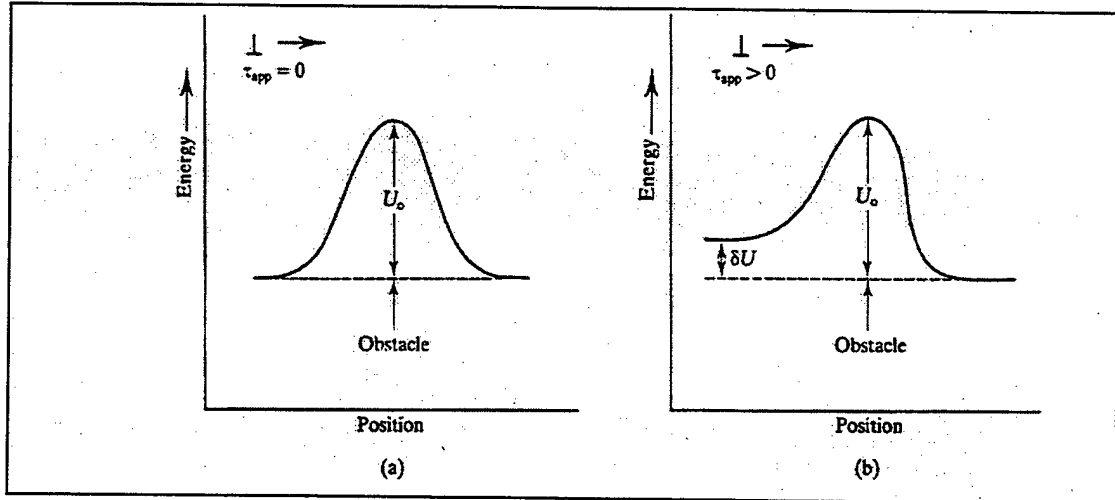
Figure 7. Schematic showing how a higher temperature helps overcome a slip plane obstacle by lowering the energy required. Diagram (a) shows the energy required to overcome the glide plane obstacle, which may be supplied either thermally or mechanically. (From Ref. 11)

1.   Dislocation Creep

Dislocation creep of a material can occur at stresses well below the yield strength of the material provided the temperature of the material is high enough (generally greater than 40% of the melting temperature for metallic materials) [Ref. 1]. Figure 7 schematically shows the effects of temperature on the ability of dislocation to pass through a glide plane obstacle. In the left schematic, it is observed that the dislocation is at the same energy level on either side of the glide plane obstacle. The activation energy Uo represents the energy that a dislocation needs to bypass the glide plane obstacle. This energy can be supplied via thermal or mechanical means. As seen in the right hand figure, the presence of an applied stress reduces the energy-position profile such that the dislocation requires less thermal energy to overcome the glide plane obstacle. As the temperature of material is raised, the amount of thermal energy to overcome a glide plane obstacle increases, and thus, a smaller stress is needed to achieve plastic flow, or creep.
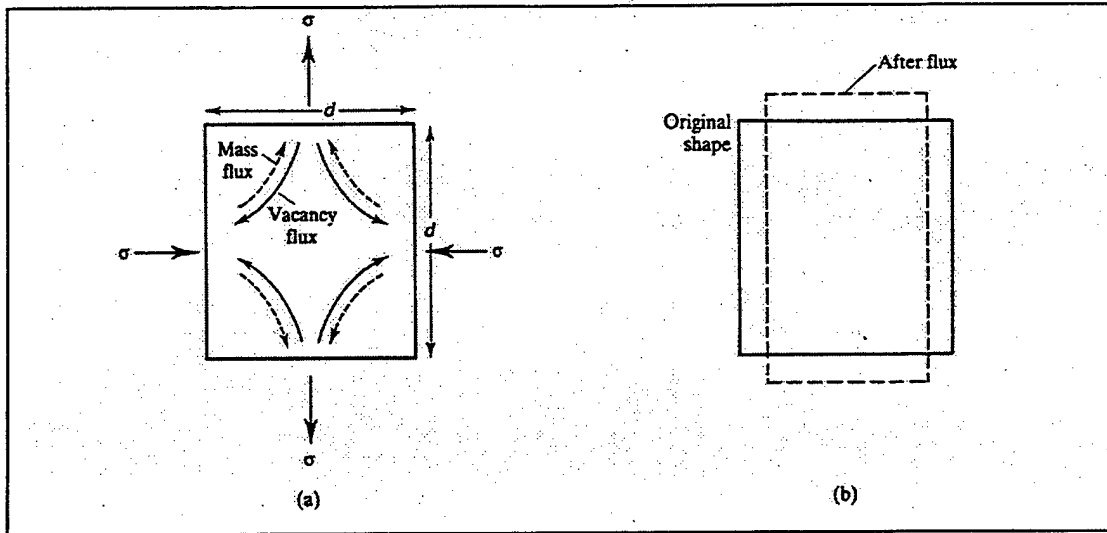
20

Figure 8. Schematic showing the diffusional Nabarro Herring creep, which occurs from a vacancy concentration gradient in a material. (From Ref. 11)

2.   Diffusional Creep

Dislocation creep involves only the flow of dislocations, and is thus necessarily restricted to crystalline materials. Creep that involves only the diffusional flow of atoms is evident in both crystalline as well as amorphous materials. Diffusional creep usually occurs under conditions of low stress and high temperature, whereas dislocation creep occurs under conditions of high stress and lower temperatures. Diffusional creep can be subdivided into two categories dependent on the path of diffusional flow.

The mechanism of Nabarro-Herring creep can be seen in Figure 8. The grain shown can be visualized as an individual grain within a polycrystal. When the lateral sides are subjected to a compressive stress and the horizontal surfaces to a tensile stress, the effective activation energy for a vacancy formation decreases in the top and bottom regions and increases near the lateral sides. Atoms now occupy some vacancies that originally existed near the lateral sides and extra vacancies begin to appear near the horizontal surfaces. A net vacancy concentration gradient thus drives the flow of

vacancies from the regions in tension to the regions in compression. There is a corresponding net mass flux from the regions in compression to the regions in tension and the grain elongates in the direction of the tensile stress. In Nabarro-Herring creep, the flow of mass occurs within the grains as seen in the figure.

The mechanism of Coble creep is similar to Nabarro Herring creep. The same vacancy concentration gradient drives Coble creep, however, the mass transport occurs along the grain boundaries of the polycrystalline material. Since the activation energy of boundary diffusion is much smaller than that of volume diffusion, it is expected that Coble creep will dominate the overall creep rate in fine-grained materials [Ref. 11]. In order to prohibit the formation of voids during diffusional creep of a polycrystalline material, some other mechanism of mass transfer must occur at the grain boundaries (Fig. 9). These additional processes of mass transfer are called *grain boundary sliding*, and mass conservation laws require that the diffusional creep rate must be exactly balanced by the grain boundary sliding rate in order to prevent void formation. The diffusional creep rate of a material is therefore governed by the smaller of the diffusional flow rate of atoms or the rate of grain boundary sliding [Ref. 11].

As discussed previously, diffusional creep is the favored mechanism under conditions of low stress and high temperatures while dislocation glide/climb is favored at higher stresses. Diffusional and dislocation creep can be considered as competitive processes with the dominant process determining the overall creep rate of the material. Diffusional creep is more important in ceramic materials than in metals due to the fact that glide/climb mechanisms are more difficult to cause in ceramics than in metals [Ref. 11].
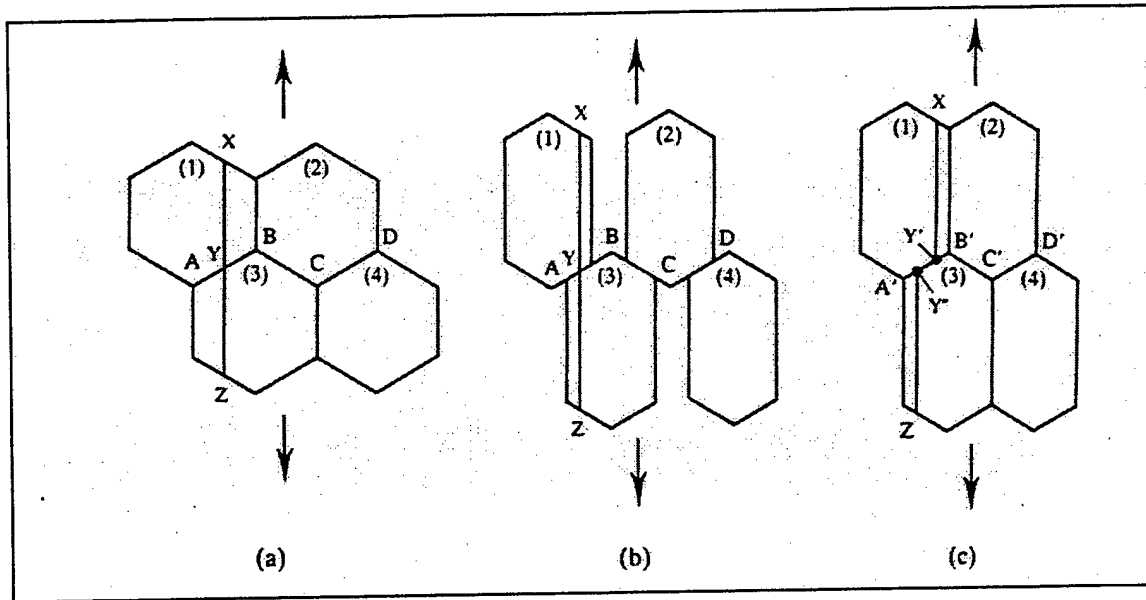
Figure 9. Schematic showing the need for some type of mass accommodation to accompany the diffusional deformation process. The accompanying mass transport occurs via grain boundary sliding in order to prevent void formation. (From Ref. 11)

D. SUPERPLASTICITY

Superplasticity is the ability of a polycrystalline material to exhibit remarkably high elongation in a generally isotropic manner in tension prior to failure at intermediate strain rates (typically 10^{-3} s^{-1}) [Ref. 2]. This phenomenon is of interest from a scientific point of view as well as from an industrial point of view due to potential applications in the materials forming industry. Superplastic deformation can be used in the production of complex shapes for which forging operations, with high strain rates, are not suitable [Ref. 11].

In general, there are two accepted methods of developing superplastic deformation [Ref. 2]. In first type called internal stress superplasticity, internal stresses generated via thermal cycling aid a small externally applied stress and cause the material to behave superplastically [Refs. 2, 12]. In structural superplasticity, a uniform, equiaxed and fine-grained microstructure is created. The grain boundaries must be high angled,

23

mobile and resist any tensile separation [Ref. 2]. Current materials forming processes require that the major emphasis be placed in the development of materials exhibiting structural superplasticity, and that mechanism is the one under consideration in this research [Ref. 2].

Microstructure plays a vital role in determining whether or not a material will be able exhibit superplastic deformation. In general, a fine grained (< 10 μm), equiaxed microstructure is required for superplastic deformation in a metallic object [Ref. 12]. The material must be highly resistant to grain growth at higher temperatures, since excessive grain growth would remove the requisite fine-grained structure [Ref. 11]. An interesting microstructural feature of a superplastic material after deformation is the grain shape. In a non-superplastic deformation, a grain generally changes shape commensurately with the overall material strain. In superplastically deformed materials, however, grain shape is essentially unchanged by the deformation [Ref. 12]. This phenomenon shows that the deformation mechanism for superplastic deformation differs from the mechanism for non-superplastic flow. The mechanism for deformation in superplasticity is widely accepted to be grain-boundary sliding with accompanying grain rotation and mass transport [Ref. 12].

1. Strain Rate Sensitivity of Superplastic Materials

The relationship between the true strain rate and flow stress of a material is given by the constitutive equation:

$$\sigma_T = \beta\left(\dot{\varepsilon}_T\right)^m \tag{3}$$

where m is the strain rate sensitivity. Superplastic behavior is usually associated with a high value of m (typically ≥ 0.3). Although the value of β can usually be considered to

be a function of strain, in superplastic behavior, this is not the case. In superplastic materials, the flow stress is independent of the strain and depends only upon the strain rate [Ref. 11]. The value of the strain rate sensitivity is determined experimentally by conducting a series of tests at constant true strain rates. The strain rate sensitivity can then be determined as the slope of the true stress versus true strain rate logarithmic plot [Ref. 12].

It has been shown, theoretically and experimentally, that the value of the strain rate sensitivity of a material is directly related to the ability of that material to resist the development of a tensile necking region during a tension test [Ref. 12]. This phenomenon can be seen theoretically by substituting $\sigma = F/A$ and $\varepsilon = (-1/A)(dA/dt)$ into equation (3) above. After substitution, we arrive at the equation:

$$\frac{dA}{dt} = \frac{-F}{\beta m} A^{m - 1/m} \tag{4}$$

As can be seen in the equation, the value of the strain rate sensitivity can realistically be bracketed between 0 and 1. A material such as a metal at a low temperature has a strain rate sensitivity of 0, and thus its flow stress has no dependence on strain rate. A material that exhibits a strain rate sensitivity of 1 also thus exhibits **dA/dt** = constant and hence, the reduction in cross-sectional area per unit time is constant. This means that when a neck forms at some location along the length of a specimen in tension, the neck will deform at the *same rate* as the material outside of the necked region [Ref. 11]. A strain rate sensitivity of 1 is representative of a Newtonian liquid for which stress and strain rate are linearly related [Ref. 13]. For any value of strain rate sensitivity less than 1, the reduction in the necked area per unit time will be greater than in regions away from the neck. A higher value of strain rate sensitivity, therefore, is indicative of a greater

25
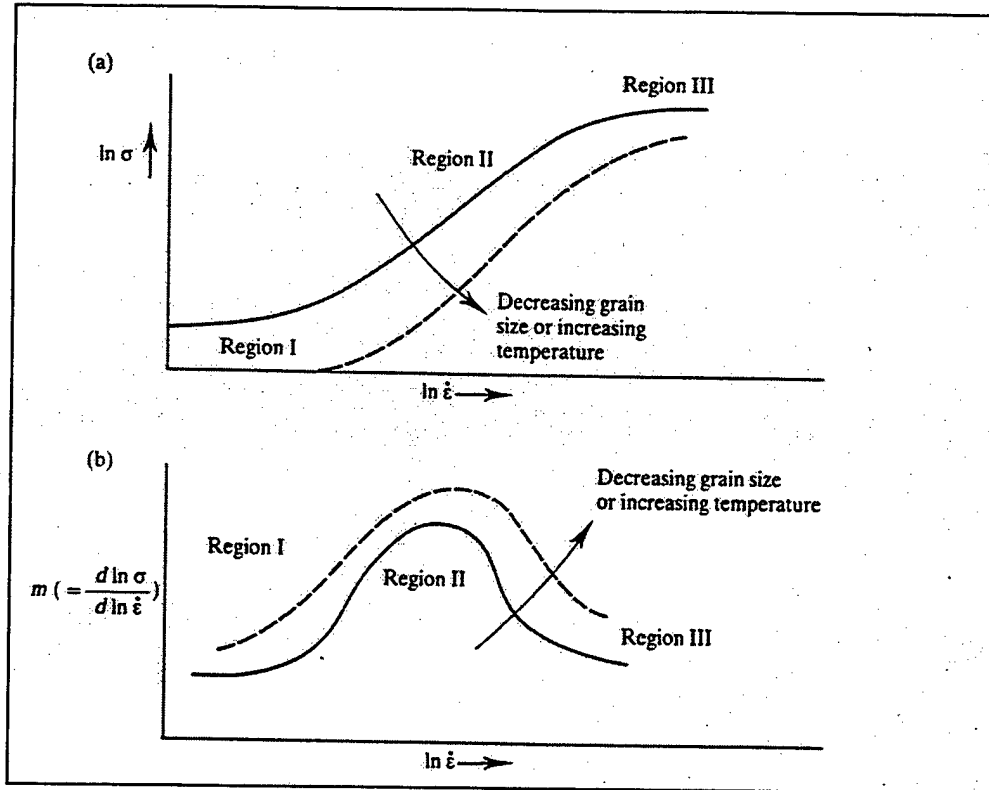
Figure 10. Schematic showing the classic sigmoidal shape of the stress-strain rate plot for a superplastic material. The strain rate sensitivity, which is the slope of the curve, is low in regions I and III, but high in the superplastic region II. (From Ref. 11)

resistance to neck development and tensile failure. A value of strain rate sensitivity greater than about 0.3 is normally associated with superplasticity [Ref. 12].

2. Experimental Observations of Superplasticity

As seen in Figure 10, the logarithmic plot of true stress versus true strain rate for a superplastic material yields a curve of a sigmoidal shape that divides the behavior into three distinct regions [Ref. 12]. As mentioned previously, the slope of this curve is the strain rate sensitivity (m) given in equation 3. The values of the strain rate sensitivities are low in both the low-stress-low strain rate region I and the high-stress-high-strain rate region III. Superplasticity, with a corresponding value of m=0.3 to 0.8 is found only in

the transition region (region II). The superplastic region is also noted to shift to higher strain rates as temperature is increased or grain size is reduced [Ref. 11].

3.   Mechanisms of Superplasticity

Many mechanisms have been proposed to explain the sigmoidal shape associated with superplasticity. Almost all of the theories agree, however, that the mechanism of deformation is grain boundary sliding accommodated by some sort of flow process. The sequential accommodation process for grain boundary sliding is provided via diffusional flow, dislocation flow or a combination of the two.

Grain boundary sliding accommodated via diffusional flow is very similar to the Nabarro-Herring and Coble creep mechanisms discussed previously. Ashby and Verall have proposed a grain-switching event that ensures the preservation of grain shape while simultaneously providing for the material deformation [Ref. 14]. Figure 11 schematically shows the grain-switching event within four grains before, after and at an intermediate stage of the process. The stress applied to the grains results in a lower activation energy for vacancy formation in the top and bottom of the grain assembly. The vacancy concentration gradient results in a net flow of mass in the direction of the applied stress and a change in grain shape. Analogous to Nabarro-Herring and Coble creep, the matter transport occurs through the grain or along the grain boundary [Ref. 15]. To preclude the formation of voids, the sequential grain-boundary sliding process discussed previously also occurs. Note that a true tensile strain of 0.55 occurs as a result of the grain switching process. As seen in the intermediate stage, an increase in grain-boundary surface area occurs when transitioning from original state and a corresponding decrease in the surface area when transitioning from the intermediate state to the final state [Ref. 11]. The

27
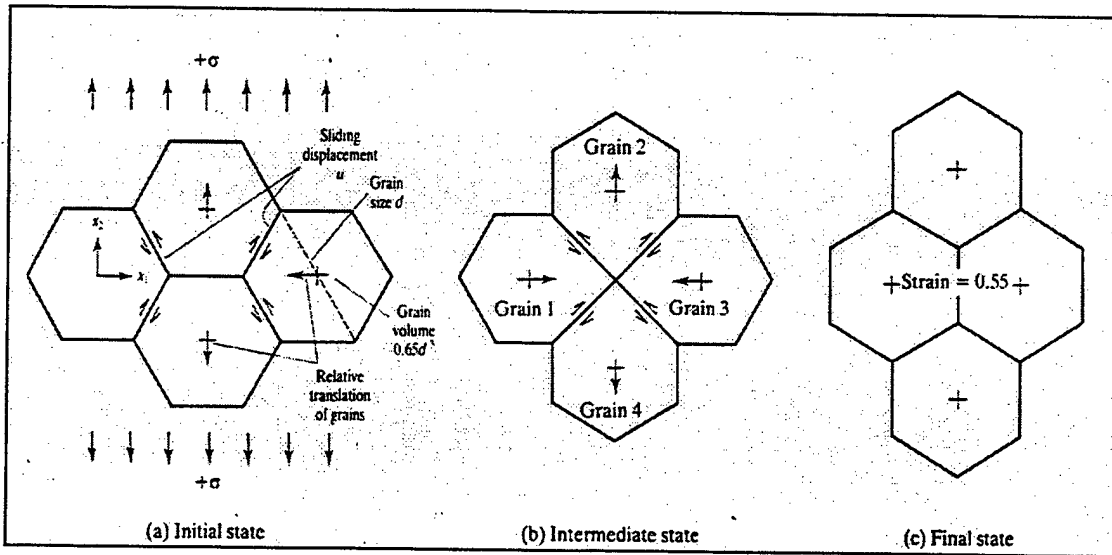
Figure 11. Schematic showing the grain switching mechanism proposed by Ashby and Verall. (From Ref. 11)

energy required to form the increased grain-boundary surface area represents a "threshold stress," below which the grain switching process cannot take place [Ref. 11]. The applied stress must perform some irreversible work to overcome the increase in surface area before the diffusional flow and grain-switching process can occur. If the threshold stress is exceeded, the strain rate for the grain-switching mechanism greatly exceeds that rate for conventional creep mechanisms. This is primarily due to the fact that, to cause a given strain utilizing grain switching, only about 1/7 of the volumetric flow of mass needs to occur as compared to pure diffusional creep [Ref. 11].

Grain-switching creep, as proposed by Ashby and Verall, occurs on a competitive process with ordinary dislocation creep. This phenomenon results in the sigmoidal shape of the stress-strain rate plot for a typical superplastic material. The grain switching process dominates in region I and dislocation creep dominates in region III. Region II, known as the transition region where both grain switching and dislocation creep occur, is characterized by a rapid increase in stress with strain rate and the corresponding

superplastic behavior. The low strain rate sensitivity in region I has been associated with the presence of impurities in superplastic alloys [Ref. 12]. As discussed previously, impurities at the grain boundaries can inhibit grain boundary sliding at low stresses and lower the achievable strain rates dramatically. Mohamed *et. al.* have shown that region I can be eliminated in the Zn-22% Al eutectoid alloy so that region II extends over several orders of magnitude of strain rate by using an alloy with 99.999% purity [Ref. 16].

4.   Contribution of Grain Boundary Sliding to Total Strain

Grain boundary sliding (GBS) plays a dominant role in superplastic deformation as evidenced by the fact that individual grains move relative to each other with little or no change in shape. Many experiments have been performed in order to determine the contribution from GBS to the total strain (ε_{gbs}), and the results have generally found that GBS accounts for more than 50% of the total strain [Ref. 12]. The remaining strain, termed "missing strain," has traditionally been assumed to be due to dislocation motion or concurrent diffusional creep of grains [Ref. 17].

Examination of experimental evidence will result in the conclusion that there is no significant strain in superplastic deformation as a result of diffusional creep. The occurrence of diffusional creep would lead to an elongation of the grains. This would be in contrast with the well-documented experimental results that grains remain equiaxed after extensive superplastic deformation [Ref. 18].

Langdon and Valiev studied the superplastic Pb 62wt.% Sn eutectic alloy at elongations of 800% and showed that the movement of intragranular dislocations occurs only as an accommodation process for grain boundary sliding, and that the net contribution to the total strain is actually close to zero [Ref. 19].

29

By examining the method of calculating the contribution of grain boundary sliding to the total strain, Langdon showed that the experimental values of ε_{gbs} =50-70% underestimate the true values of GBS contribution. This error was determined to be due to limitations in the measuring procedure, and Langdon concluded that essentially all of the strain in superplastic deformation is the result of grain boundary sliding [Ref. 17].

E.   SUPERPLASTICITY OF CERAMICS

The intense scientific study of superplasticity began in the 1960s. The study of superplasticity in ceramics and ceramic composite materials, however, is of very recent origin. This is primarily due to the fact that ceramics normally fracture intergranularly at low strain values due to their weak grain boundary cohesive strength [Ref. 20]. Wakai *et. al.* stunned the scientific community on July 5, 1985 when they reported that they had demonstrated superplasticity in a yttria-stabilized tetragonal zirconia polycrystalline material (3Y-TZP) at the Government Industrial Research Institute in Nagoya, Japan [Ref. 12]. Since their discovery, a number of fine-grained polycrystalline ceramics have been shown to have superplastic capabilities (eg., Al_2O_3/Y_2O_3, Hydroxyapatite, β-Spodumene glass) [Ref. 20]. As mentioned previously, a grain size on the order of 1 μm is usually required for superplasticity in ceramics [Ref. 2].

A general question that has yet to be answered is whether or not the presence of a grain boundary glassy phase is required for superplasticity in ceramics [Refs. 2, 20]. Many microstructural studies have been carried out in YTZP in an attempt to answer this crucial question. Nieh and Wadsworth have demonstrated over 800% elongation in their YTZP with no glassy phase present at the grain boundaries [Ref. 21]. Although the presence of a glassy phase at the grain boundaries of a fine grained ceramic may not be a

prerequisite for superplasticity, its presence can remarkably enhance the process of grain boundary sliding. Wakai et.al., for example, have shown that by doping TZP with manganese oxide in order to create a grain boundary glassy phase, the temperature required to achieve superplastic deformation can be substantially reduced [Ref. 20].

As discussed previously, a value of strain rate sensitivity greater than about 0.3 is associated with superplastic behavior. In the literature, there is considerable disparity in the value of the strain rate sensitivity reported for 3Y-TZP, the *m* value ranging from 0.3 to 0.5 [Ref. 20]. Impurity content and microstructural evolution during superplastic deformation have been proposed to explain the discrepancies in the reported values of strain rate sensitivity [Refs. 2,20]. Nieh and Wadsworth showed that concurrent grain growth with superplastic deformation could result in artificial effects on the determination of *m* values [Ref. 20]. By normalizing the stress with the square of the final grain size, they show that the actual strain rate sensitivity exponent of all samples is about 0.67 [Ref. 20]. Carey was the first to point out that the value of strain rate sensitivity is proportional to the Al_2O_3 content in YTZP [Ref. 22]. The values of *m* for samples with high (.065%) Al_2O_3 content were 0.5, while the values for samples with low (0.005%) Al_2O_3 content were 0.3. This finding again suggests that a grain boundary glassy phase promotes superplastic deformation [Ref. 22].

F.   DEFORMATION IN THE PRESENCE OF A LIQUID PHASE

Creep deformation in the presence of a liquid phase has been utilized for many years. Skiers rely on the plasticity of wet snow to achieve great speed and control while dentists depend on the interim plasticity of amalgam in order to properly set fillings in a

cavity [Ref. 7]. Sintering, although different from creep, involves similar mass transport mechanisms and is accelerated by the presence of a liquid phase [Ref. 7].

The mechanism by which a liquid containing solid will deform is dependent upon the relative amount of liquid phase present. A viscous liquid containing solid particles deforms and exhibits large elongations via rheological flow, not superplasticity [Ref. 15]. The term superplasticity as applied to ceramics, therefore, should only be used when the volume fraction of the glassy phase is less than a few percent. For solids that contain a large volume fraction of glassy phase (> 10 vol %), rheological flow is the governing deformation mechanism [Ref. 15].

Polycrystalline solids with a small amount of liquid phase present at the grain boundaries deform by grain boundary sliding via solution-precipitation creep. The liquid phase acts as a medium for mass transport by allowing solution and reprecipitation of the solid phase [Ref. 15]. Since applied tensile stresses are present during superplastic forming, the grain boundaries must be able to support tensile loading. In the case where there is a continuous liquid phase at the grain boundary, this leads to the inference that the grain boundary liquid phase can support a normal tensile stress without cavitating prematurely in order for the material to behave superplastically [Ref. 23]. Clarke has shown that this assumption is justified for a small amount of grain boundary glassy phase and normal deformation stresses. This is due to the fact that interatomic forces develop between the solid a liquid layer immediately adjacent to the solid suitably oriented to provide some normal load bearing capability [Ref. 24]. Ultimately, whether or not a material with a liquid phase at the grain boundary will exhibit superplasticity is dependent on both the amount and distribution of the liquid phase within the solid

skeleton. A very thin layer of grain boundary liquid, or clean grain boundaries with the liquid concentrated primarily in pockets at triple grain junctions are generally thought to be conducive to superplastic forming by resisting cavitation at the grain boundary, which eventually limits tensile ductility [Ref. 25]

G. PROPOSED PROCESS WINDOW FOR FORMING OF CERAMICS DURING LPS

The manufacture of ceramic products with complicated shapes is often prohibitively expensive due to the post fire machining process that is required to produce the final shape. As discussed, when a ceramic product is manufactured, the ceramic powder is sintered to allow densification and strengthening of the green compact. The use of a liquid phase at the grain boundary can increase the rate of sintering and lower the required temperature. The deformation mechanism of a liquid containing solid has also been discussed and it is believed that a solid with a small amount of liquid phase present at the grain boundaries deforms by grain boundary sliding via solution-precipitation creep through the liquid phase.

Combining the sintering process and liquid phase enhanced deformation to achieve net-shaped products is the goal of the present study. The sintering process will be allowed to occur without applied stress until the rearrangement stage is over. The compact will be allowed to sinter into stage two, and *contact flattening* via diffusional flow near stress concentrations will be allowed to progress. The stress will be applied part way through stage two, when *Ostwald Ripening* has not yet become the dominant deformation mechanism. The deformation phase will thus take place concurrently with *Ostwald Ripening* in stage II of the sintering process, with deformation occurring via

33

grain boundary sliding by solution-precipitation mass transport in the liquid phase. The solid state sintering process will then be allowed to take place in order to strengthen the net-shaped product produced.

III. OBJECTIVES OF THE PRESENT STUDY

The objective of the present study is explore the suitability of SiO_2-B_2O_3 as a model system for liquid phase sintering (LPS) with SiO_2 as the solid (high melting) phase and B_2O_3 as the liquid (low melting) phase. Using this system, which allows processing at relatively low temperatures and in air, the phenomenon of liquid phase sintering and deformation in the presence of a liquid phase are combined. The goal of the LPSF process is to form a net-shaped product in one manufacturing step. In addition to studying the suitability of the model system for study of LPS, a preliminary investigation of the deformation behavior of the SiO_2-B_2O_3 system with various levels of B_2O_3 above its melting point is investigated.

IV. EXPERIMENTAL METHODS

A. SELECTION OF A MODEL SYSTEM

The B_2O_3-SiO_2 system was chosen for study of the LPSF process (Fig. 12). As seen in the phase diagram of the system, B_2O_3 is the low melting temperature component (T_m=450 °C) and SiO_2 is the high melting temperature component (T_m=1710 °C). The system was chosen due to its favorable properties for the LPSF operation. B_2O_3 has almost no solubility in SiO_2, but SiO_2 has a solubility of approximately 5 wt % in liquid B_2O_3 at 460 °C. This is expected to allow the solution-reprecipitation mechanism of the LPS process to be operative since it is above the melting point of the eutectic. Powder compacts having a high weight percentage (95-99 wt %) of SiO_2 and a small weight percentage (1-5 wt %) of B_2O_3 were made utilizing powder consolidation and compaction techniques discussed previously.

At low temperatures, the powder mixture will be composed of large particles of SiO_2 surrounded by particles of B_2O_3. As the temperature is raised, the compositions and concentrations of the constituents remain the same until the melting point of the eutectic composition is reached, whereupon a small amount of liquid B_2O_3 is formed. The composition of this liquid rapidly changes to the composition C_E, as dictated by the phase diagram. At this point, solid SiO_2 is in equilibrium with a liquid of composition C_E. The relative amounts of SiO_2 and eutectic liquid are given by the lever rule:

$$W_{SiO_2} = \frac{C_E - C_B}{C_E} \tag{5}$$

$$W_L = \frac{C_B}{C_E} \tag{6}$$
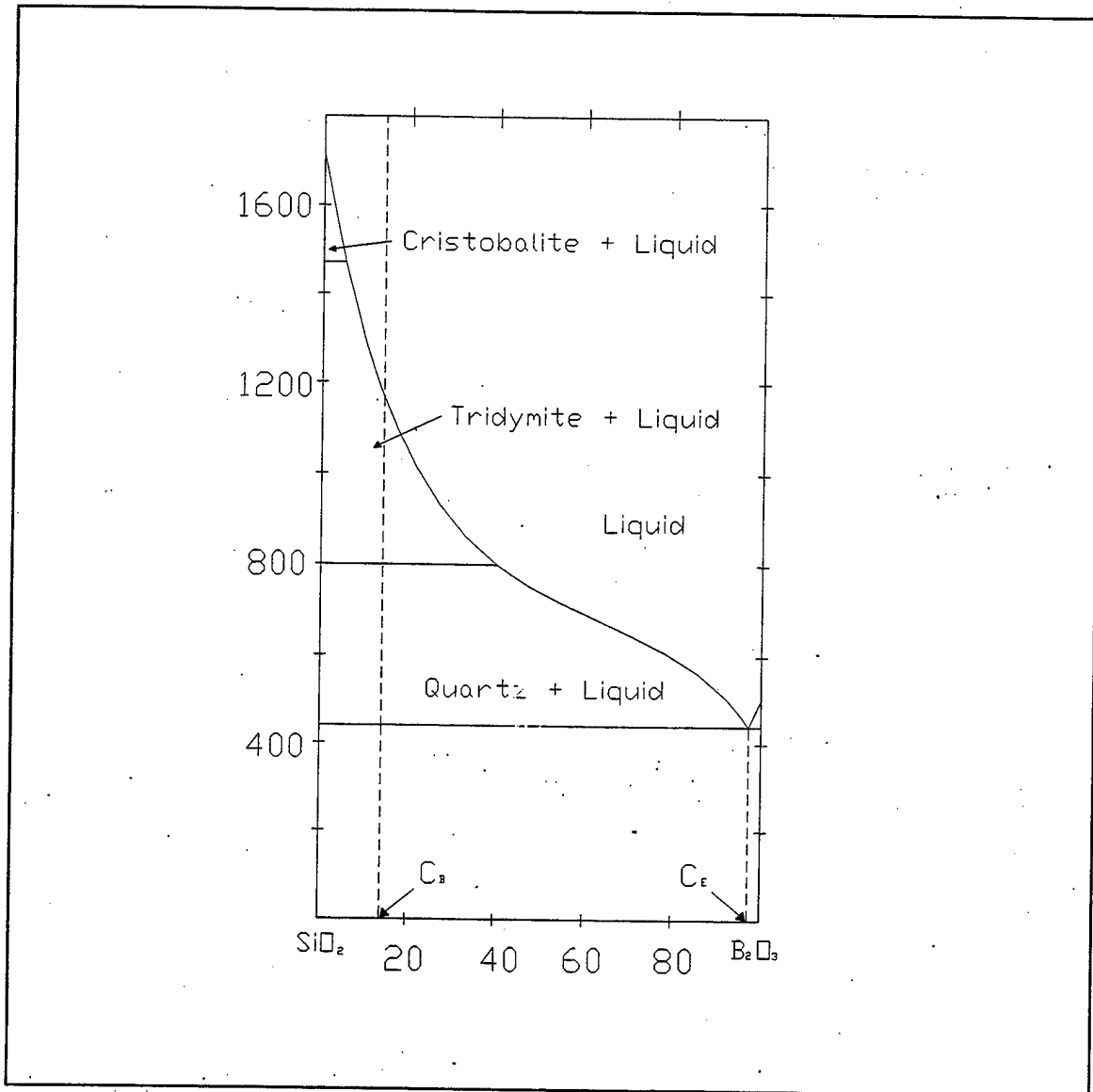
Figure 12. Phase diagram for the SiO_2-B_2O_3. C_E and C_B note the eutectic and overall composition of the SiO_2-B_2O_3 mixture respectively. (After Ref. 28)

Initially, sintering of the compact at the specified temperature is allowed to occur without deformation in order to allow for the particle rearrangement stage of LPS to result in initial densification. Once the solution-reprecipitation stage has commenced, the compact is simultaneously sintered and compressed in order to study the deformation characteristics. By careful control of the time of sintering prior to deformation, the effects of porosity level may be evaluated.
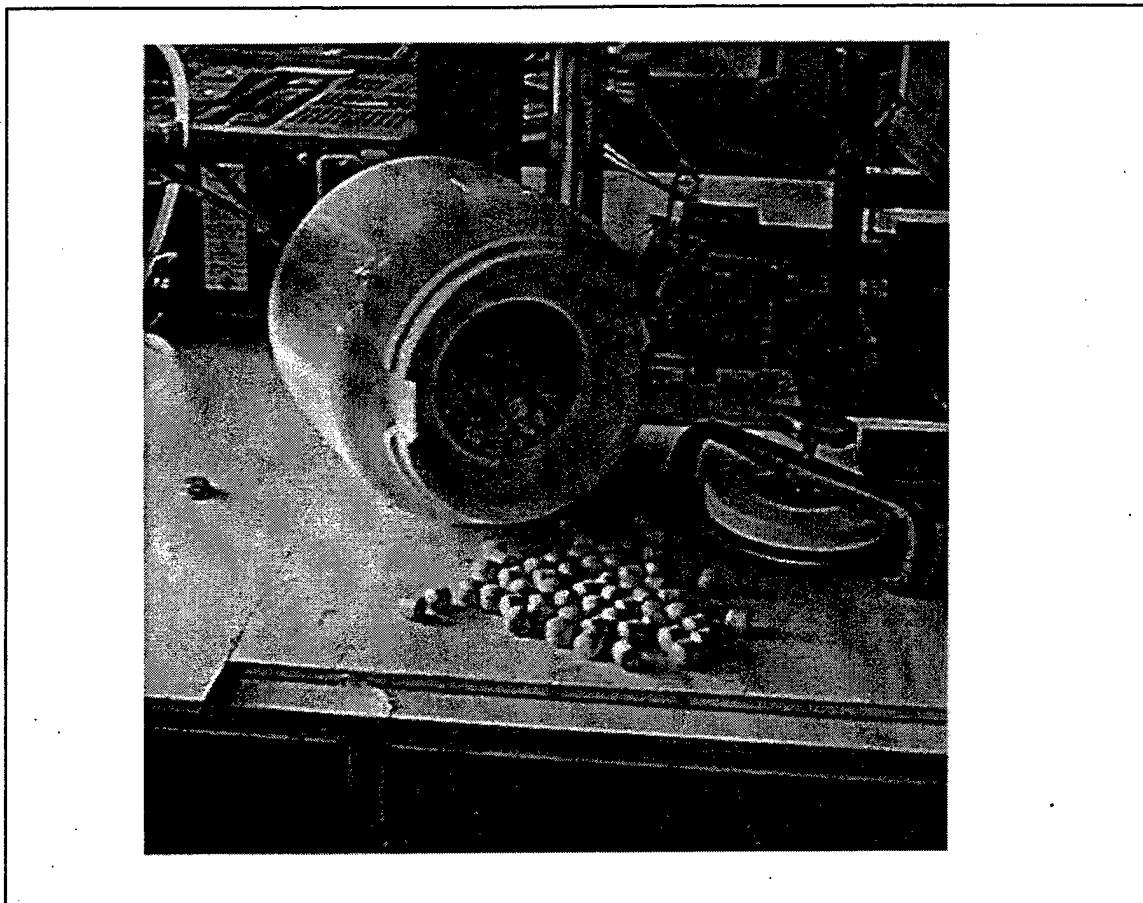
Figure 13. A picture of the ceramic cylindrical ball mill and zirconia grinding media used for powder sizing and mixing.

B.   EXPERIMENTAL

1.   Powder Processing

a.   *Powder Selection, Sizing and Mixing*

Silicon Dioxide with a purity of 99.6% and a –325 mesh sizing was purchased from Aldrich chemical company. An alumina–fortified porcelain jar, zirconia grinding media and a single tier ball mill were utilized for powder sizing and mixing (Fig. 13). The jar was filled to 55% of its total volume with the zirconia grinding media prior to powder loading.

The SiO_2 powder was mixed with methanol and milled for 72 hours in order to effect a particle size reduction. After milling, the resulting slurry was poured onto a tray and the methanol was boiled off at a temperature of 70 °C for thirty minutes. The sized SiO_2 powder was mixed with several additives in preparation for the consolidation stage. Three weight percent Polyvinyl Alcohol (PVA) was chosen as the binder for the system and three weight percent Polyethylene Glycol (PEG) was selected as the lubricant. The binder and lubricant were mixed in with the sized SiO_2 powder along with 1-5 weight percent B_2O_3 via wet milling in methanol for 24 hours. The resulting slurry was poured out of the milling jar onto a tray, and the methanol was boiled off at 70 °C for one hour. A temperature of 70 °C was chosen for evaporating methanol due to the fact that the binder, Polyvinyl Acetate, has a glass transition temperature of 79 °C. The resulting flaky mixture was ground by hand using a mortar and pestle.

In one case, a powder mixture consisting of SiO_2, 10 wt % B_2O_3, 3 wt % PVA and 3 wt % PEG was dry milled after sealing the jar in a nitrogen atmosphere. This procedure was utilized to minimize the moisture level in the mixture and thereby reduce contamination and concomitant coagulation of B_2O_3, which is hygroscopic. As discussed subsequently, this approach was intended to provide a more uniform distribution of B_2O_3 relative to that available via wet milling.

b.   *Powder Consolidation*

A simple cylindrical punch and die made of stainless steel was utilized to construct the sample powder compacts (Fig. 14). Approximately 10 grams of powder was compacted in each batch to produce a cylindrical compact with an aspect ratio of about 2. The internal surfaces of the die and punch system were painted with a
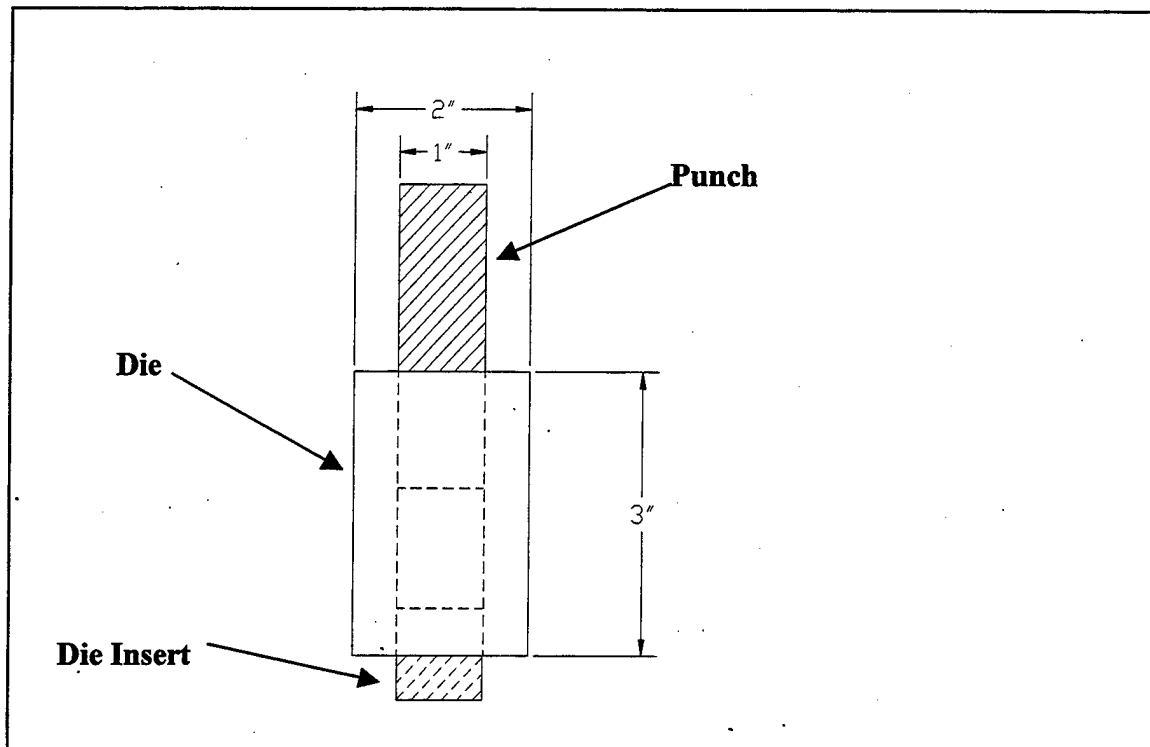
Figure 14. A schematic diagram showing the dimensions of the punch and die used for making the powder compacts.

suspension of Molybdenum Di-Sulfide (MoS_2) in methanol for lubrication purposes. The die was allowed to stand at room temperature following application of the suspension until the methanol evaporated, leaving a thin film of the lubricant on the die walls.

A SATEC ™ model 20UD materials testing system was utilized to perform the consolidation of the powder compacts in the die-punch system described above (Fig. 15). A computer program was utilized to maintain a constant pressure of 150 MPa on the punch for a period of 2 hours at ambient temperature. The two-hour time limit was allowed to ensure uniform compaction of all samples. Following compaction, the samples were removed from the die utilizing a hand press ejection pin and stored for subsequent sintering and/or testing.
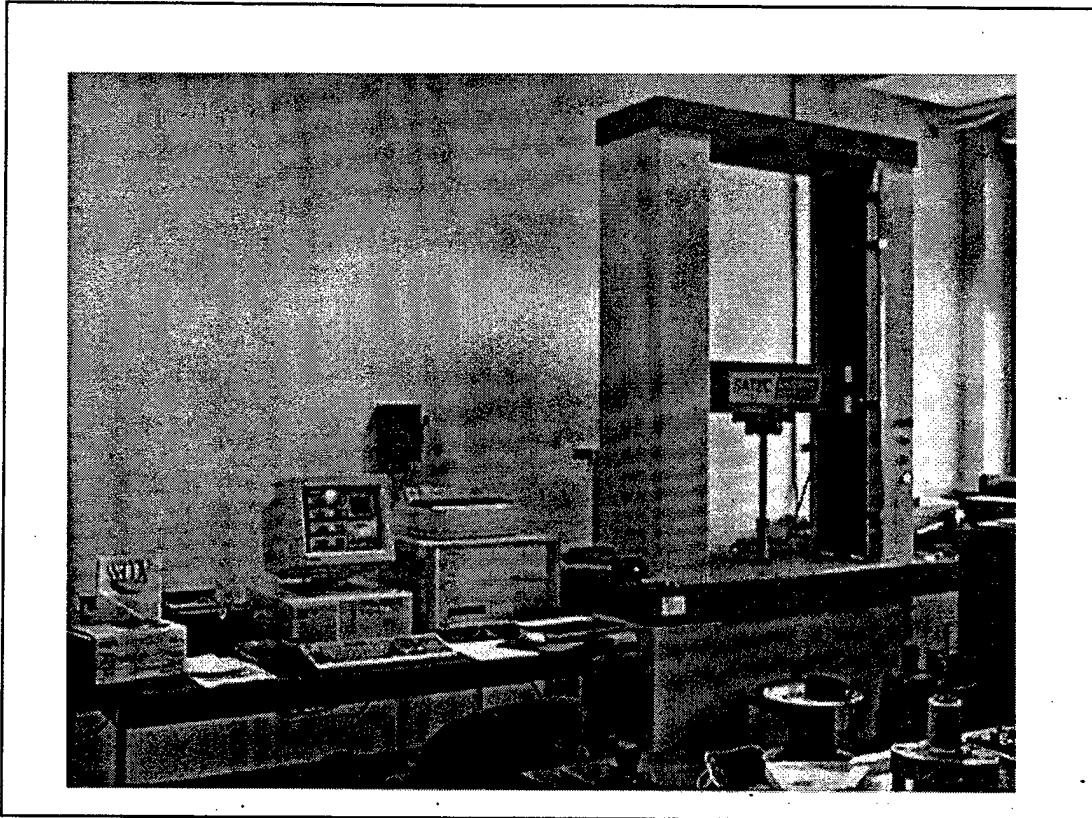
Figure 15. A picture of the SATEC Model 20UD materials testing system as set up for the compaction process. The computer system was programmed to maintain a constant pressure of 150 MPa on the punch for two hours in order to achieve uniform density.

2.   Liquid Phase Sintering

Some of the compacts were sintered at various temperatures in order to determine

the effects of Liquid Phase Sintering without concomitant deformation. Densities were

determined by measuring the dimensions of the compacts and their mass prior to

sintering. The compacts were placed in an oven at room temperature and heated to 130

^{0}C at a rate of 40 ^{0}C/min. The compacts were then heated to 150 ^{0}C at a rate of 2 ^{0}C/min

in order to allow the PEG, which has a flash point of 159 ^{0}C to evaporate. The

temperature was subsequently raised to 560 ^{0}C at a rate of 40 ^{0}C/min and held at the

sintering temperature for a period of 12 hours.

After the 12 hour sintering period, the oven was turned off and the sample was allowed to cool in the furnace to room temperature. Densities were again determined by measuring the dimensions of the sintered compacts and their mass. More accurate density measurements were then determined utilizing Archimedes' method. The force measurements were made in air and Johnson's ™ baby oil, and the calculations discussed previously were made to determine density. The density of the baby oil was provided by the manufacturer and verified by measurements of the weight of 10 ml of the baby oil as measured by a graduated cylinder. In order to prevent any of the baby oil from penetrating the surface of the compact, the compact was coated with a thin layer of wax prior to the density measurements.

3.   Deformation of Compacts During Liquid Phase Sintering

A schematic diagram of the testing system constructed can be seen in Figure 16. The connecting bolts and threaded fasteners were made of construction grade steel. The push rods and pressure plates were constructed of Inconel Alloy X-750. Alloy X-750 is precipitation hardened alloy of Nickel and Chromium with Titanium and Aluminum additions for precipitation hardening [Ref. 26]. The desirable properties are:

1. Good corrosion resistance

2. Good tensile strength and creep resistance

3. Can use in temperatures up to 700^0C

The furnace used for heating was purchased from Watlow Ceramic Fiber Heaters. The heater is a split tube type heater with an inner diameter of 5 inches, an outer diameter of 9 inches and a length of 18 inches. Rated at 240 volts and 1775 watts, the heater is
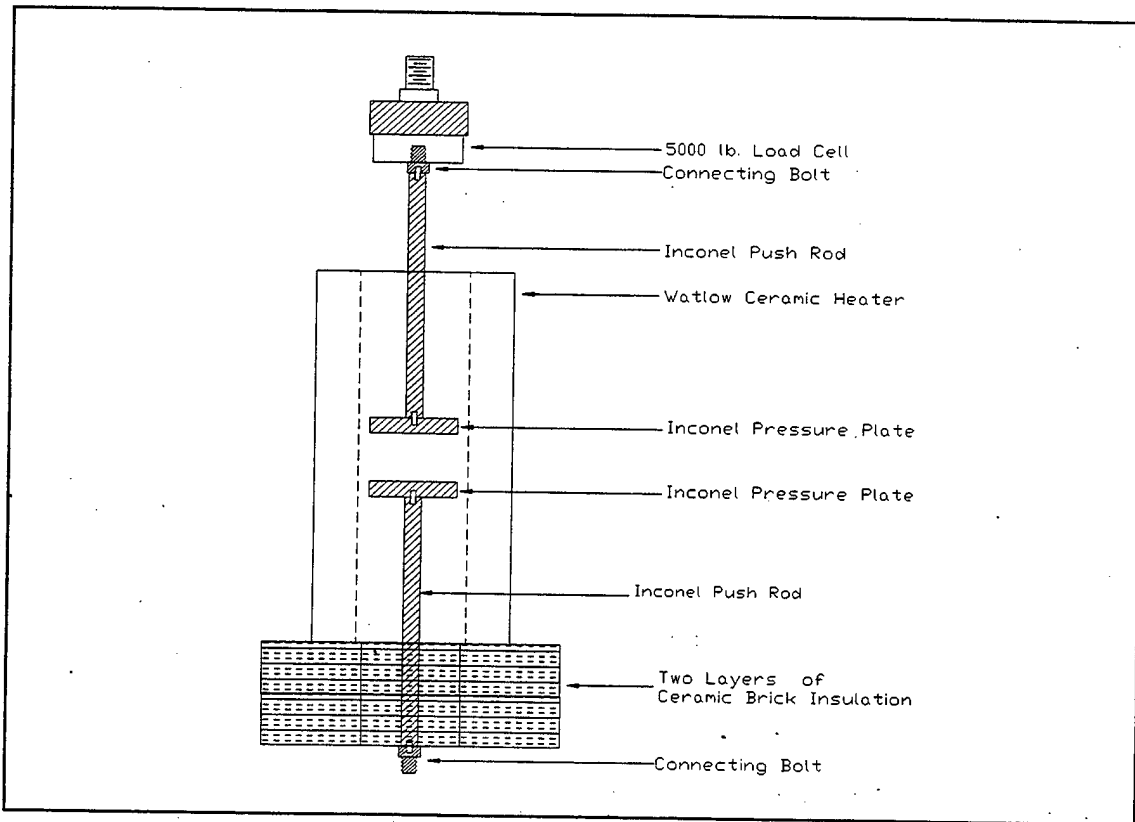
Figure 16. A design schematic of the compression assembly.

made of an alumina-silica composition and held together by an inorganic binder which

allows operation at temperatures up to 1204 °C.

As shown in the schematic and picture of the testing system, the split tube heater

was placed on two layers of insulating bricks in order to protect the surface of the testing

platform (Fig. 17). The bottom push rod was attached to the base of the materials testing

machine and the top push rod was fastened to a 5000-pound load cell, which was itself

attached to the testing machine. The surfaces of the Inconel pressure plates, as well as

the top and bottom surfaces of the powder compact, were painted with a suspension of

Molybdenum Di-Sulfide (MoS_2) in methanol for lubrication purposes. The pressure

plates and compact were allowed to stand at room temperature following application of

the suspension until the methanol evaporated, leaving a thin film of high temperature

44
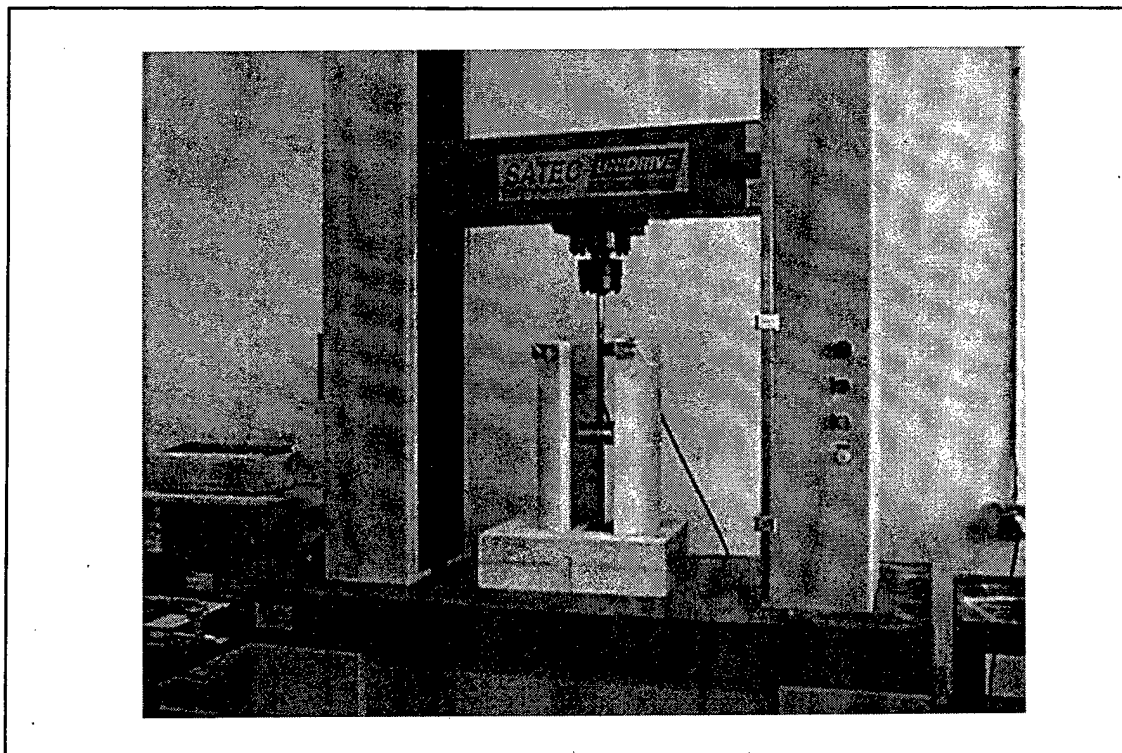
Figure 17. A picture of the liquid phase sinter forming compression test apparatus that was constructed for testing compression of liquid containing solids.

lubricant on the surfaces. The sample was then placed on the bottom pressure plate and the top push rod and pressure plate were lowered until there was a 1mm clearance between the top of the compact and the pressure plate. The gap was left to allow for thermal expansion of the compact and the Inconel components during heat up to testing temperature. The heater was then closed and energized.

Two thermocouples were built into the system, with one in each of the pressure plates. Holes with a 1/16 " diameter were drilled into the pressure plates to house the thermocouples. The thermocouples were each attached to the heater controller for sensing and feedback loops. The temperature of a bucket of ice water was measured by each thermocouple to ensure proper calibration and operation. The system temperature was raised at a set point ramp rate of 3 ^{0}C/min to a temperature of 150 ^{0}C, where it was

held for 30 minutes in order to allow the evaporation of the PEG, which has a flash point of 159 ^{0}C. The temperature was raised to 220 ^{0}C at 3 ^{0}C/min and held there for 15 minutes in order to allow for the decomposition of PVA. The samples were then heated to 460 ^{0}C at 3 ^{0}C/min and allowed to sinter for three hours in order to allow time for stage I and part of stage II of LPS to occur.

After the three-hour sintering period, a compressive load was applied to the compact via the top pressure plate at a nominally constant true strain rate, obtained by varying the crosshead velocity as a function of time over 40 discrete data points. These programmed velocities were determined for each test utilizing the desired true strain rate, the initial compact height, and the final compact height. The load as measured by the load cell was recorded as a function of time and stored in ASCII data files for further analysis and stress strain plots.

4. X-Ray Diffraction

The starting powders as well as the sintered powder mixture of SiO_2 and B_2O_3 were analyzed via X-Ray Diffraction (XRD). The samples were first ground into fine powders using mortar and pestle, sized via a 100 μm sieve and then mounted on glass slides with amyl-acetate. An even coating of powder was sprinkled onto the glass slide, and the excess was wiped off prior to performing the XRD analysis. A goniometer controlled by a DEC VAX workstation was used to examine the samples (Fig. 18). The scans were taken from 10 ^{0} to 40 ^{0} (2θ) in increments of 0.05 ^{0} and time steps of 2 seconds.
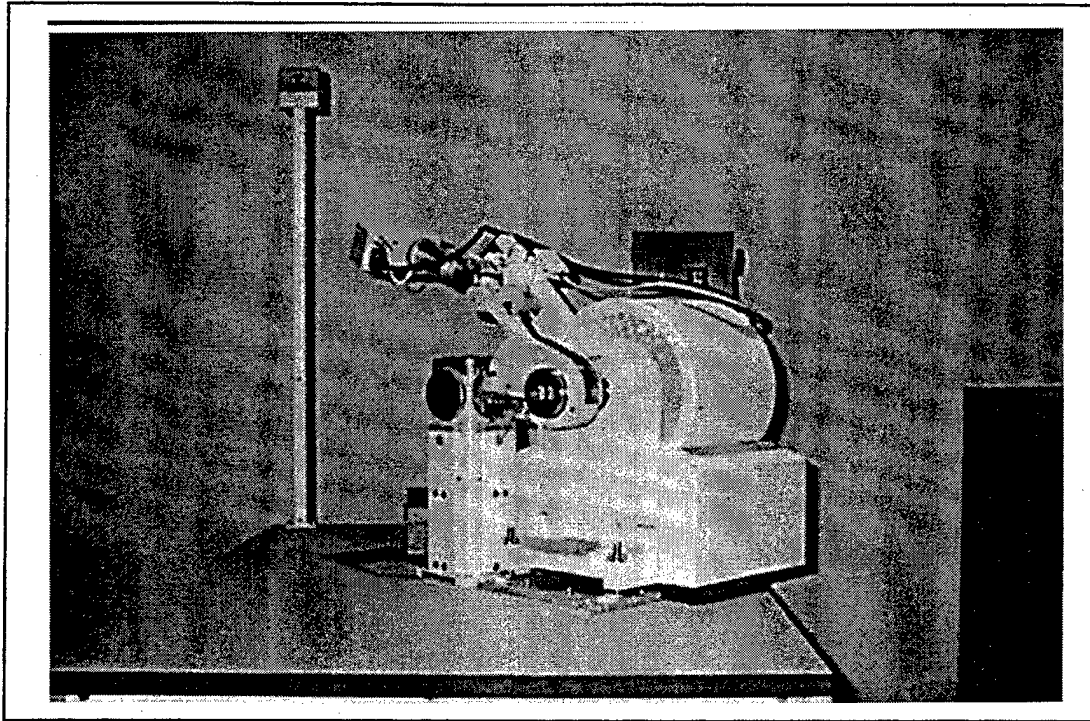
Figure 18. A picture of the goniometer used for X-Ray Diffraction analysis of powders and powder compacts.

5.   Scanning Electron Microscopy (SEM)

The starting SiO_2 powder and the fracture surface of one sample were examined

via Scanning Electron Microscopy (SEM). The SiO_2 powder was milled for 72 hours in a

solution of methanol and dried for 3 hours at 70 ^{0}C to evaporate the methanol. Some of

the powder was then suspended in a solution of methanol and ultrasonically vibrated for

one hour in order to prevent particle agglomeration. The solution was then placed on

double-sided carbon tape and the methanol was allowed to evaporate leaving only fine

grains of powder. The powder sample was mounted in a Topcon SM-510 SEM (Fig. 19)

and micrographs were taken in order to qualitatively ascertain the particle size.

The fracture surface of a sintered sample was also studied using SEM and Energy

Dispersive X-ray Analysis (XRD) using the Topcon SM-510. Since the ceramic is non-

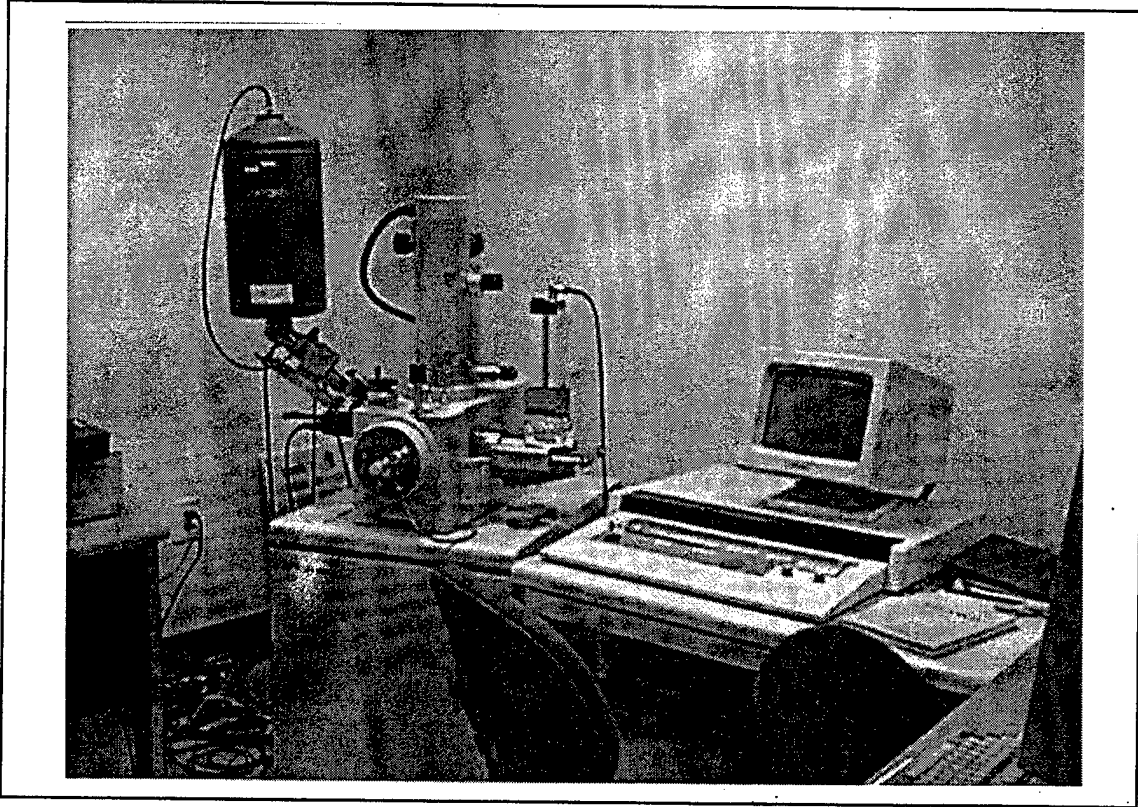conducting, the fracture surface was carbon coated by vacuum evaporation and the

Figure 19. A picture of the TOPCON SM-510 Scanning Electron Microscope used for SEM and EDX analysis.

remainder of the compact painted with a carbon solution prior to loading in the SEM.

Micrographs were taken of the fracture surface to ascertain porosity levels and EDX was performed on the fracture surface in order to view the distribution of B_2O_3 on the surface.

V. RESULTS AND DISCUSSION

A. POWDER PROCESSING AND SINTERING

1. XRD and SEM Analysis of Powders

Analysis of the SiO_2 and B_2O_3 starting powders in as purchased condition was performed via x-ray diffraction (XRD) analysis. As seen in Figure 20, the diffraction patterns produced, which show that the Bragg diffraction condition is satisfied by some set of crystallographic planes, are the same as the JCPDS patterns for SiO_2 powder. Since B_2O_3 is hygroscopic and absorbs CO_2, the powder was heated to 250 ^{0}C in order to eliminate these compounds (H_2O and CO_2), and XRD was performed on this powder (Fig. 21). The diffraction pattern found for the B_2O_3 was found to match the JCPDS card for $(B_2O_3)80C$, a cubic polytype of boron oxide (JCPDS card number 6-297). One of the sintered 5 wt % B_2O_3 compacts was fractured and pulverized using a mortar and pestle. This powder was also analyzed using XRD, and the peaks corresponding to boron oxide and silicon dioxide starting powders are present (Fig. 22).

Scanning electron microscopy (SEM) was performed on the SiO_2 powder after sizing in order to determine the particle sizes and size distribution. The micrograph shown in Figure 23 shows that the particle sizes range from sub-micron level to sizes on the order of a few microns. As discussed earlier, for superplasticity in ceramics, two prerequisites are that the particle sizes must be on the order of 1 micron, and that a range of particle sizes is required. The SEM analysis thus revealed that the particle sizes and size distribution were adequate for superplastic forming.
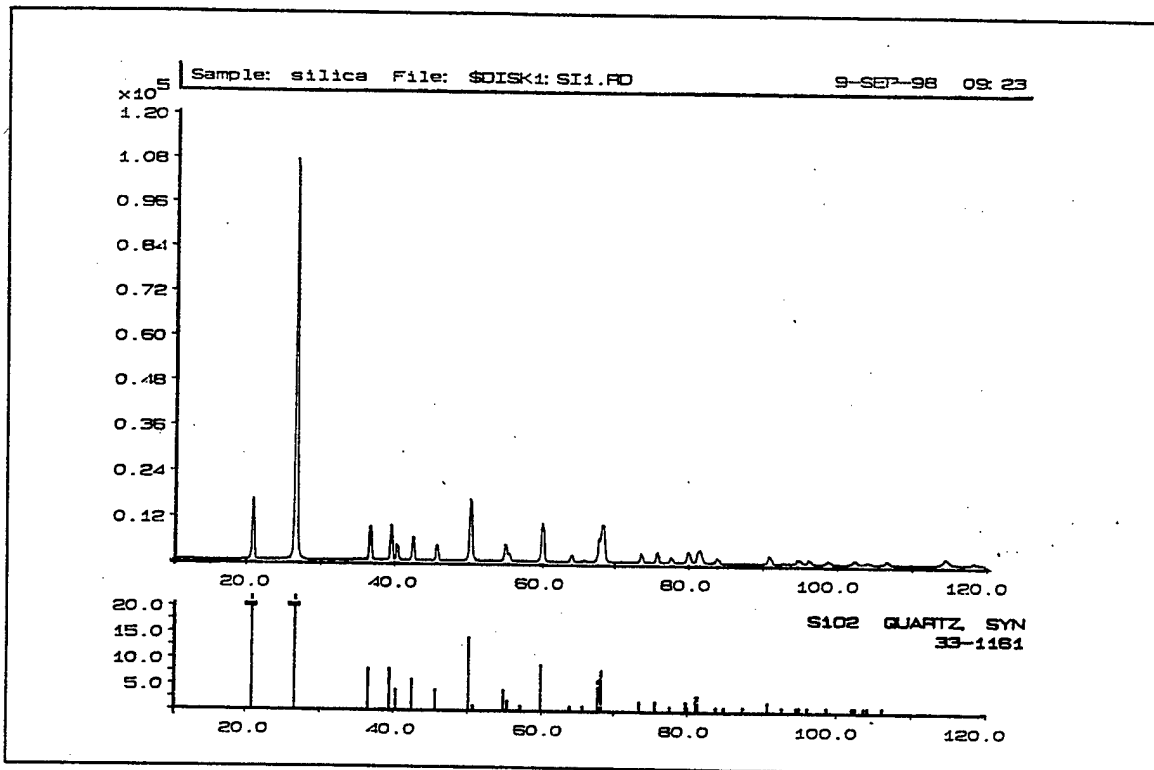
49

Figure 20. X-Ray diffraction pattern of SiO_2. Note the close agreement between the diffraction peaks and those shown on the JCPDS card.
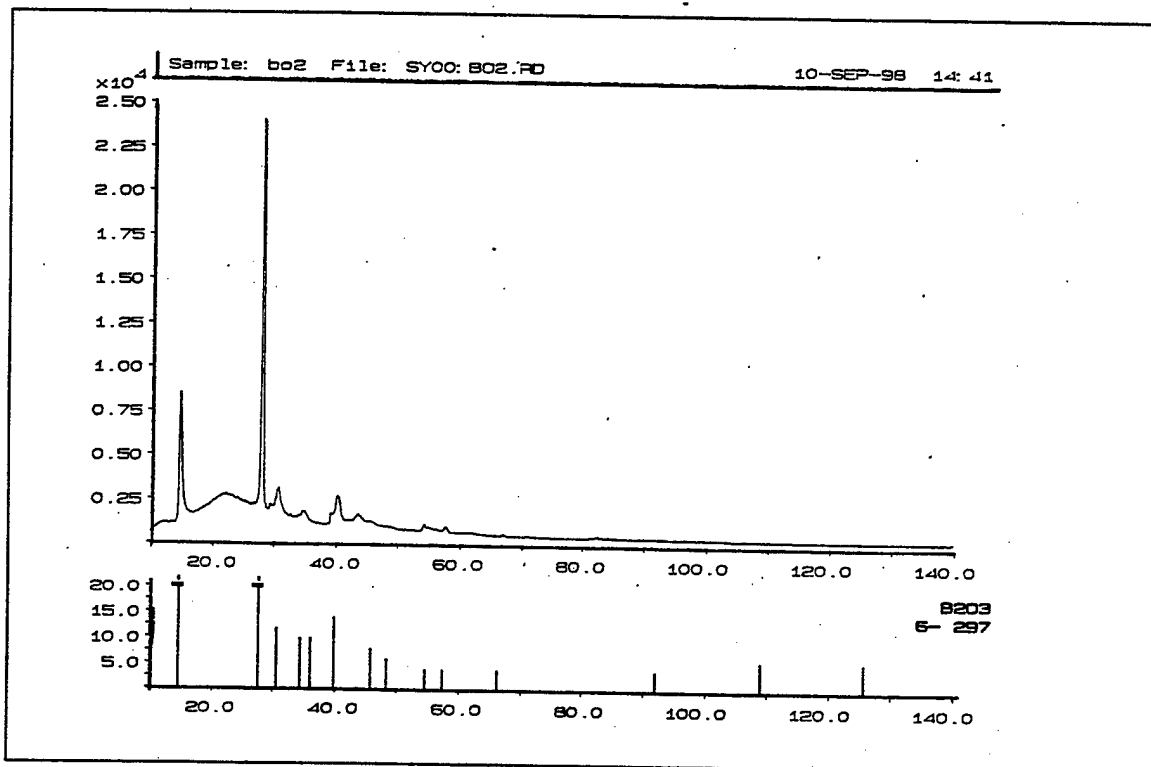

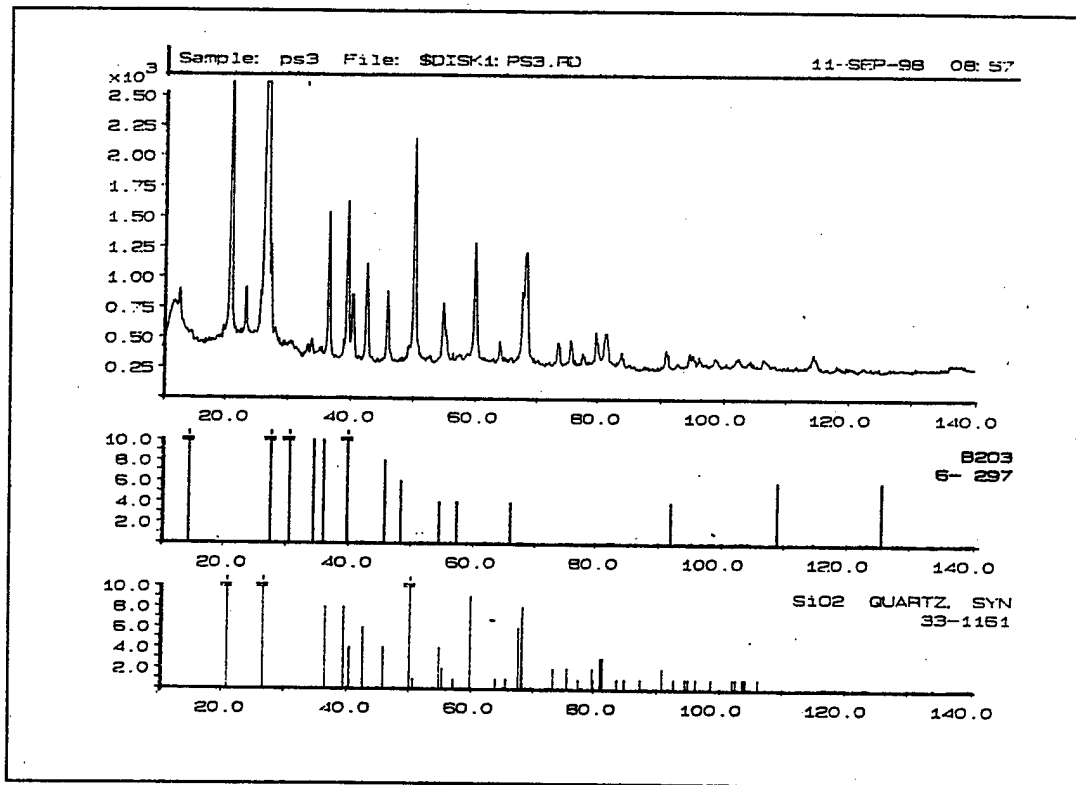**Figure 21.** X-Ray diffraction pattern of B_2O_3 after processing to remove dissolved H_2O and CO_2.

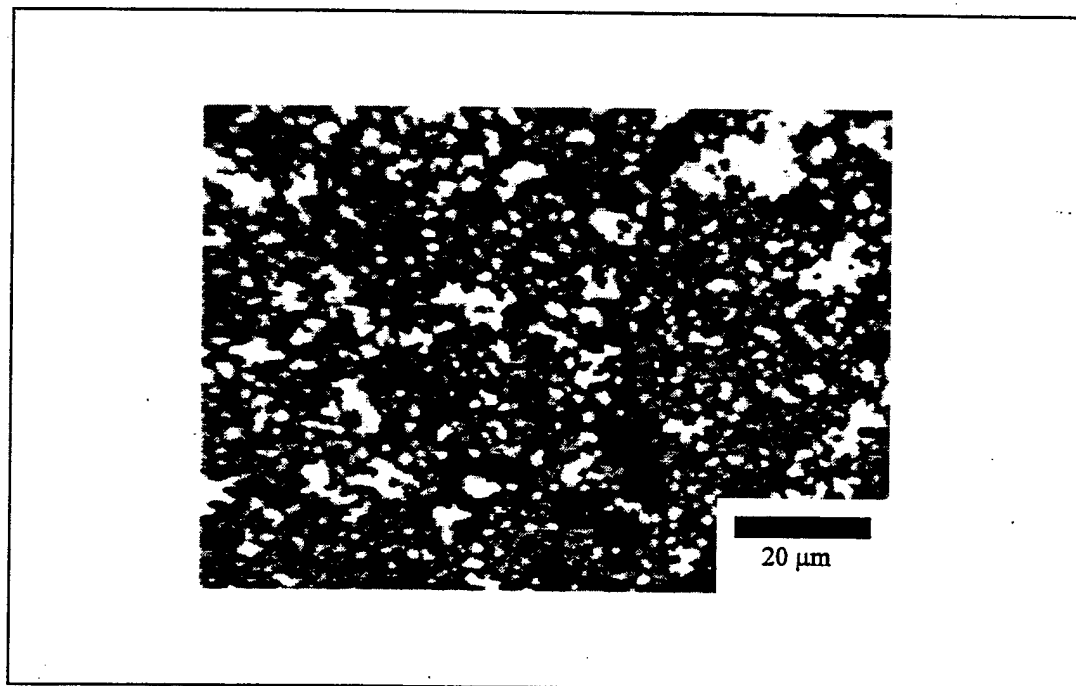**Figure 22.** X-Ray diffraction pattern of sintered SiO_2 - 5% B_2O_3 powder compact.

Figure 23. Micrograph of the starting SiO_2 powder showing the size distribution.

2. Density Measurements of Sintered Compacts

The relative densities of various compacts were determined before and after the sintering process as discussed previously, and the results of the measurements are summarized in Table 1. The theoretical density of each of the compacts was determined using a rule of mixtures calculation, assuming that the density of SiO_2 is 2.65 g/cm^3 and the density of B_2O_3 is 2.46 g/cm^3. The sintered compact densities were then compared to the theoretical density in order to determine the relative density of the sintered compacts. As expected, the 5 wt % B_2O_3 sample compacted at 150 MPa has a higher green density and sintered density than the sample compacted at the lower pressure. The samples that were sintered at the higher temperatures also show a higher sintered density, indicating that some liquid phase sintering is taking place. The densities of the as sintered compacts are not, however, representative of a fully densified ceramic but indicative of significant porosity.

Sample	wt % B_2O_3	$P_{compaction}$ (Mpa)	T_{sinter} (^0C)	$\rho_{theoretical}$ (kg/m^3)	ρ_{green} (kg/m^3)	$\rho_{sintered}$ (kg/m^3)	$\rho_{relative}$ (%)
1	5	88	470	2.639	1.250	1.373	52
2	5	150	470	2.639	1.371	1.456	55
3	1	150	560	2.648	1.373	1.570	59.3
4	5	150	560	2.639	1.370	1.550	58.7
5	10	150	560	2.630	1.375	1.578	60

Table 1. Table showing the relative densities of the sintered compacts as functions of weight percent B_2O_3 present, compaction pressure and sintering temperature. The relative densities shown are for the sintered compacts.

Sample number 4 was fractured by impact, and scanning electron microscopy was performed on the fracture surface. Since the ceramic is non-conducting, the fracture surface was carbon coated and the remainder of the compact painted with a carbon solution prior to loading in the SEM. As expected, SEM analysis indicated significant porosity on the fracture surface (Figs. 24, 25). EDX was also performed, and no B_2O_3 was detected at any location on the fracture surface.

It is well known that a given material will fracture along its weakest strength cross-section when subjected to impact loading. Having no indication of B_2O_3 on the fracture surface indicates a failure of the B_2O_3 to adequately flow around the SiO_2 grains, and the sample would predictably fail on a weak surface where no LPS had occurred (i.e., on a surface with no B_2O_3 present). The lack of LPS near the fracture surface is attributable to the inability of the B_2O_3 to distribute itself uniformly throughout the interstices of the SiO_2 powder, thus preventing any of the stages of LPS from occurring except in the regions where B_2O_3 was coagulated.

In order to determine why B_2O_3 did not penetrate all the interstices of the SiO_2 powder mass and thereby gave inadequate LPS, a small about of B_2O_3 powder was placed in a SiO_2 test tube and heated to 560 ^{0}C. Shortly after the system reached equilibrium, the oven was opened and the test tube was visually inspected. The liquid B_2O_3 was observed to have climbed up the walls of the test tube (Fig. 26), suggesting that the solid SiO_2-air surface energy is significantly greater than that for the liquid B_2O_3-solid SiO_2 interface. Thus, excellent wetting of SiO_2 by liquid B_2O_3 is displayed at 560 ^{0}C. This suggests that lack of wetting is not responsible for the non-uniform distribution of B_2O_3 obtained in the compact.
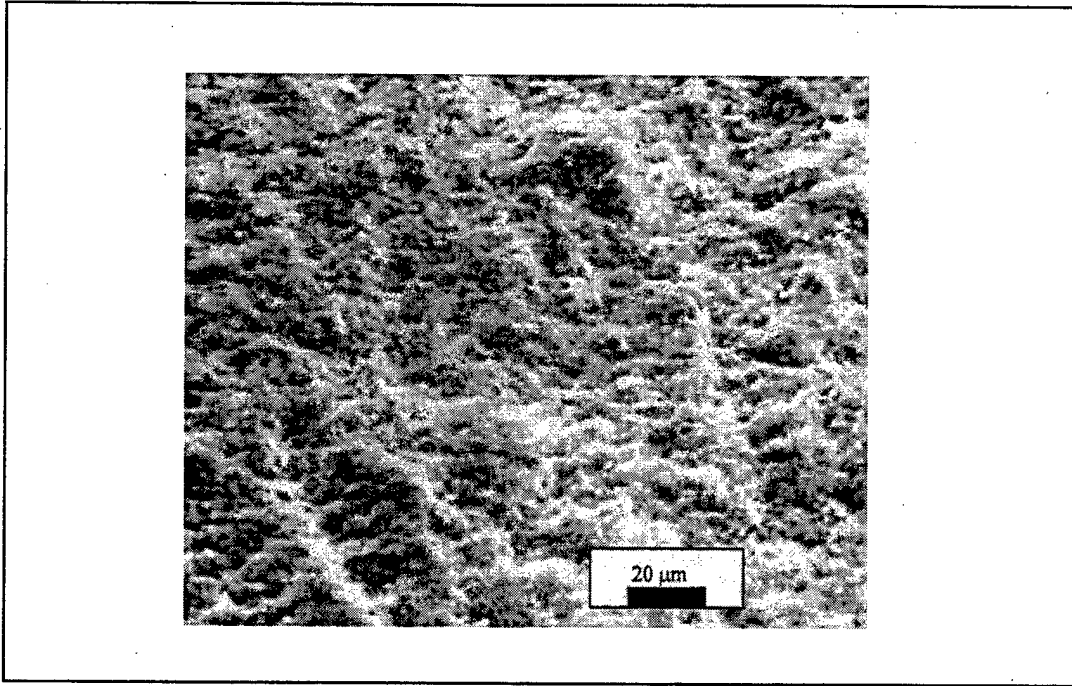
Figure 24. Scanning electron microscope (SEM) micrograph showing severe porosity along the fracture surface of the sample number 4.
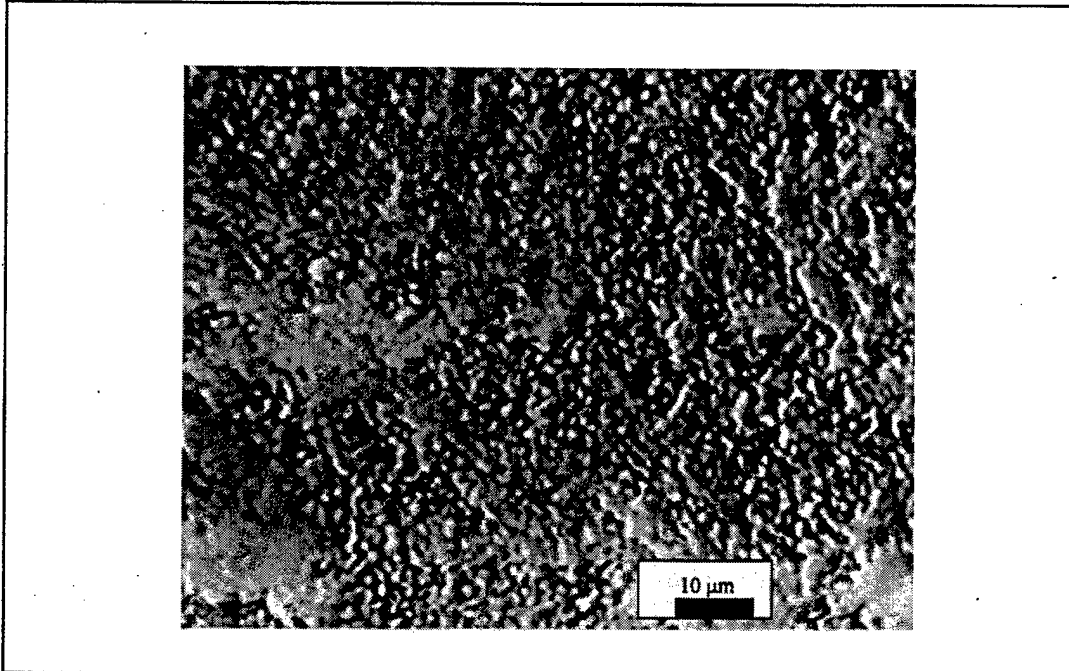
Figure 25. Higher resolution scanning electron microscope (SEM) micrograph showing severe porosity along the fracture surface of the sample number 4.
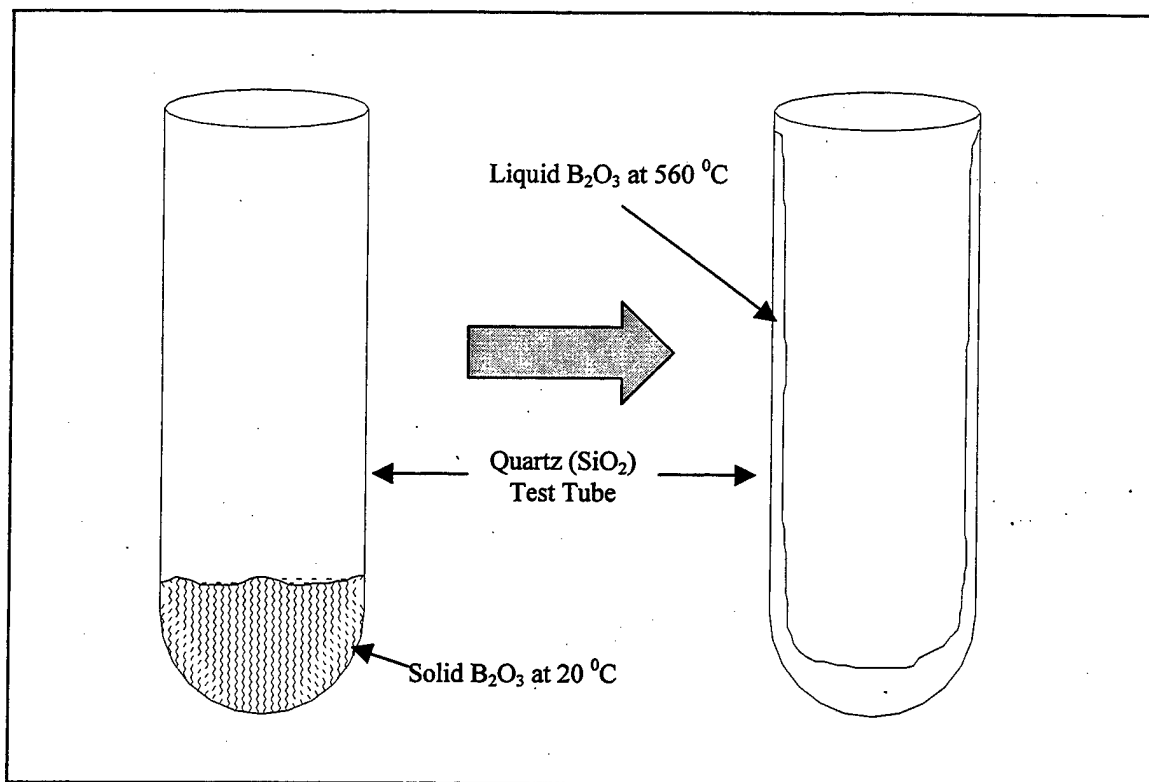
Figure 26. A schematic showing the solid B_2O_3 in the Quartz (SiO_2) test tube at room temperature and the excellent wetting of SiO_2 by B_2O_3 once the temperature of the test tube is raised above the melting temperature of B_2O_3.

In order to determine whether interaction between B_2O_3 and Polyethylene Glycol may have caused the B_2O_3 to coagulate in localized areas of the compact, a sample of B_2O_3 powder was placed on a petri-dish in the laboratory, and a drop of PEG was placed on the boron oxide. The PEG was quickly absorbed into the B_2O_3 and a mixture with the consistency of model glue was formed. It was thus determined the absorption of the lubricant (PEG) by the sintering aid (B_2O_3) formed a very viscous, non flowing liquid, which prevented the uniform distribution of B_2O_3 among the particles of SiO_2 during the powder mixing stage prior to compaction. It was thence determined that all future processing should be done with solid lubricants only so that B_2O_3 can be properly distributed in the compact.

B. DEFORMATION OF SINTERED COMPACTS

Deformation of some compacts in the presence of a liquid phase was performed utilizing the compression apparatus designed and constructed (Figs. 17, 18). Initial trial experiments indicated overall sample failure at strain rates of approximately 18-20%, and the total testing strain for subsequent tests was predetermined to be 16%. Presetting the overall strain allowed programming the crosshead velocity as a function of strain so that a nominally constant true strain rate could be maintained throughout the test. Typical tests revealed significant (~16%) deformation for the ceramic compacts. This is shown in Figure 27, which plots the nominal true stress vs. the nominal true compressive strain for a nominally constant applied true strain rate of 5×10^{-4} s^{-1}. Although the outer areas of the compacts were crushed during the test, central portions of the compacts remained intact and did not fracture. Figure 28 shows a photograph of the compact prior to deformation, as well as appearance of the sample after deformation. During deformation, much of the exterior portions of the sample (which were not adequately sintered) crumbled, leaving only the well sintered solid inner core (which presumably had an adequate amount of B_2O_3) capable of undergoing deformation.

Although some of the deformation of the unsintered parts during compression may be due to densification, it is believed that a significant fraction of the 16 % strain is attributable to high temperature deformation mechanisms within the compact. This is reasonable since, in the absence of die-wall constraints on the sides of the compact during compression, an unsintered, porous compact would be expected to collapse immediately. The fact that in the present case, significant deformation of the core of the compact was observed in the absence of overall disintegration suggests that the compact is capable of
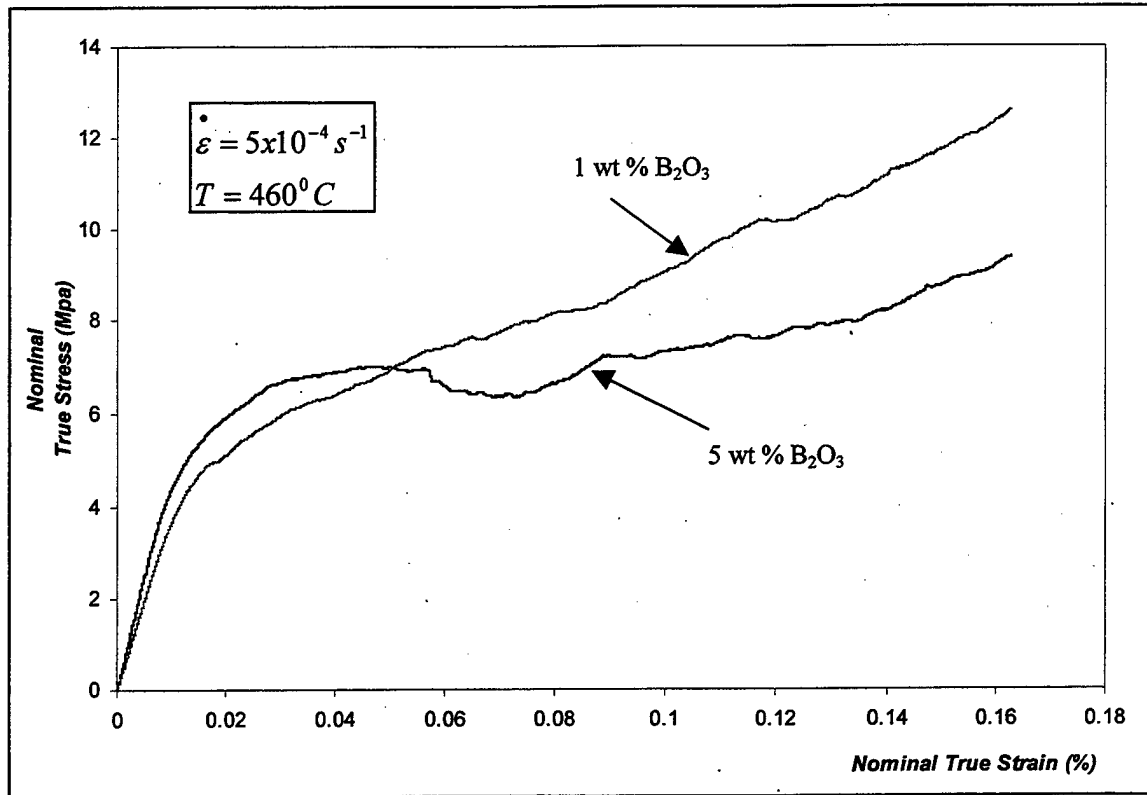
Figure 27. Nominal true stress vs. true strain for the SiO_2 compacts with 1 weight percent and 5 weight percent B_2O_3 respectively. Both tests were performed at temperatures of 460 °C and nominally constant true strain rates of 5 x 10^{-4} s^{-1}.
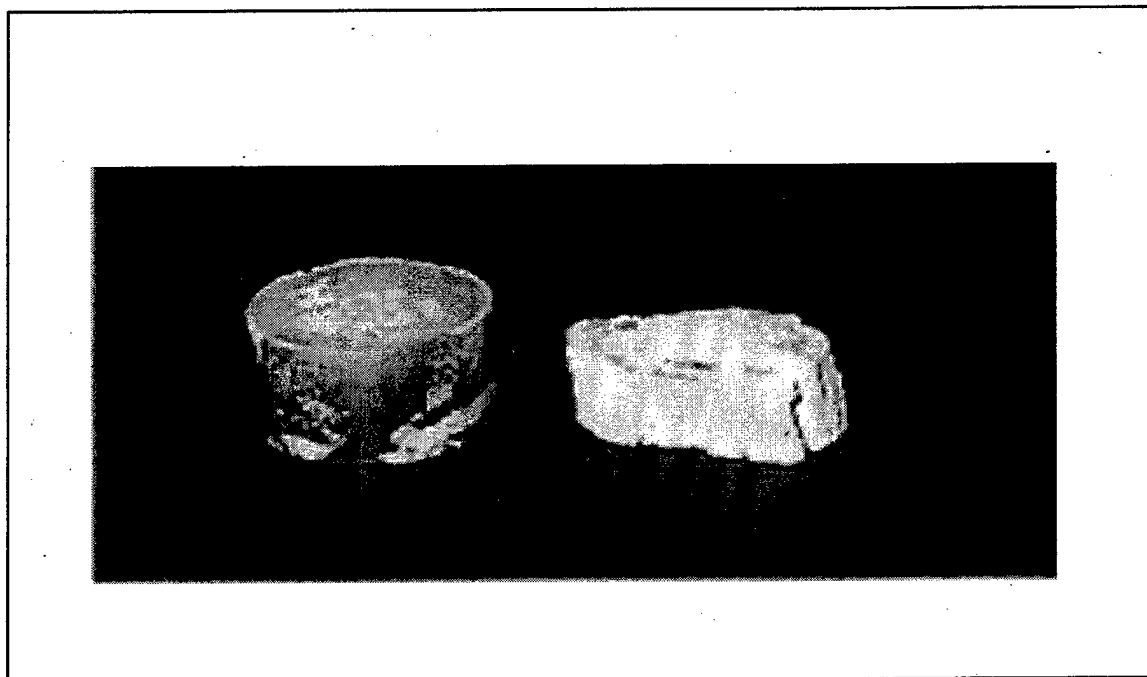
Figure 28. A picture of a sintered compact beside a compact that underwent 16% deformation. Note that although the outer surfaces fractured, the inner core is still solid.

deforming via mass transport through the liquid phase. Based on the above results, it appears likely that the coagulation of B_2O_3 due to absorption of PEG led to poor distribution of B_2O_3 in SiO_2. Despite excellent wetting of SiO_2 by B_2O_3, the B_2O_3 was unable to penetrate all of the interstices of the SiO_2 particles throughout the compact, and remained concentrated only in localized regions. These regions would presumably have close to theoretical density, and therefore, showed significant deformation strains (~16%) without fracture at temperatures where B_2O_3 is liquid; whereas the other parts of the compact which were devoid of B_2O_3 collapsed and/or fractured.

VI. CONCLUSIONS AND RECOMMENDATIONS

The goals of this study were to evaluate the $SiO_2 - B_2O_3$ model system for suitability for Liquid Phase Sintering and to perform a preliminary investigation of the deformation behavior of the system with various percentages of B_2O_3 above its melting point. Scanning Electron Microscopy (SEM), Energy Dispersive X-Ray Analysis (EDX) and X-Ray Diffraction Analysis (XRD) were used to analyze the powders employed for sample formation and the resulting sintered compacts. Deformation of the compacts at elevated temperatures seemed to show some dependence on the amount of liquid phase present, although the failure to achieve a uniform distribution of the sintering aid obviously prevented a full analysis of the proposed Liquid Phase Sinter Forming process.

Adequate densification of the compacts was not achieved during sintering, indicating that the Liquid Phase Sintering process did not occur as expected. The coagulation of the sintering aid (B_2O_3) in certain areas of the compact and failure to distribute uniformly around the grains was determined to be the cause for the lack of LPS. The coagulation of the B_2O_3 was determined to be caused by its ability to absorb the lubricant used in the system (Polyethylene Glycol) to form a mixture of glue-type consistency which would not adequately flow and evenly mix with the SiO_2 powder during milling. This lack of uniform mixing precluded LPS from occurring everywhere within the compact.

The parts of the compacts which were infiltrated with the liquid B_2O_3, however, showed significant deformation at temperatures above the melting point of B_2O_3. Although some of the deformation was probably attributable to densification of the porous compacts, it is believed that a significant fraction of the observed 16%

59

deformation is attributable to deformation enhanced rapid mass transport through the liquid phase via a grain boundary sliding mechanism. It is therefore concluded that the $B_2O_3 - SiO_2$ system shows promise as a model system for studying the processes of Liquid Phase Sintering (LPS) and Liquid Phase Sinter Forming (LPSF) provided the B_2O_3 phase is evenly distributed throughout the SiO_2 powder mass during the preconsolidation mixing stage. The apparent affinity of B_2O_3 to absorb water and other organic liquids (e.g., Polyethylene Glycol, Methanol) suggests that a dry lubricant must be used in order for the B_2O_3 to be adequately dispersed. It is therefore recommended that a dry lubricant such as zinc stearate or sodium stearate be utilized for all future tests.

LIST OF REFERENCES

1. Calister, William, *Materials Science and Engineering. 2nd ed.*, John Wiley and Sons, Inc., 1991.

2. Neih, T.G., J. Wadsworth and F. Wakai., "Recent Advances in Superplastic Ceramics and Ceramic Composites." *International Materials Review*, **36:** pp. 146-161, 1991.

3. German, Randall M. *Sintering Theory and Practice.* John Wiley and Sons, INC., 1996.

4. Lenel, F.V. *Powder Metallurgy, Principles and Applications.* Metal Powder Industries Federation, 1980.

5. Richerson, David W., *Modern Ceramic Engineering, Properties, Processing and Use in Design. 2nd ed.*, Marcel Dekker Inc., 1992.

6. Glass, S.J. and K.G. Ewsuk. "Ceramic Powder Compaction," *Compaction Science and Technology MRS Bulletin*, pp. 24-28, 1977.

7. G. M. Pharr and M.F. Ashby, "On Creep Enhanced by a Liquid Phase" *Acta. Metall.*, **31:** p.129, 1983.

8. Klar, Erhard, ed., *Metals Handbook, Volume 7, Powder Metallurgy*, American Society for Metals, 1984.

9. Mahoney, F.M. and M.J. Readey. "Ceramic compaction Models: Useful Design Tools or Simple Trend Indicators?" (Unpublished manuscript).

10. Blumenthal, W.R., H. Scheinberg and S.A. Bingert, "Compaction Issues in Powder Metallurgy," *Compaction Science and Technology MRS Bulletin*, p. 32, 1977.

11. Courtney, Thomas H., *Mechanical Behavior of Materials*, McGraw-Hill Publishing, New York, 1990.

12. Chokshi, A.H., Mukherjee, A.K, and T.G. Langdon, "Superplasticity in Advanced Materials," *Materials Science and Engineering*, **R10:** pp. 237-274, 1993.

13. White, Frank, *Fluid Mechanics*, McGraw-Hill Inc., 1994.

14. M.F. Ashby and R.A. Verall, "Diffusion –accommodated flow and Superplasticity," *Acta. Metall.*, **21:** pp.149-163, 1973.

15. F. Wakai, N. Kondo, H. Ogawa, T. Nagano and S. Tsurekawa, "Ceramics Superplasticity: Deformation Mechanisms and Microstructures," *Materials Characterization*. **37**: pp. 331-334, 1996.

16. Chaudhury and F.A. Mohamed, *Acta. Metall.*, **36**:1099, 1988.

17. Langdon, Terence G, "An evaluation of the strain contributed by grain boundary sliding in superplasticity," Department of Materials Science and Mechanical Engineering, University of Southern California, 1993.

18. Nagano, Takayuki, Sawao Honda, Fumihiro Wakai, and Mamoru Mitomom, "Compressive Deformation of Liquid-Phase Sintered Silicon Carbide at Elevated Temperature," *Superplasticity and Superplastic Forming*, pp. 247-255, 1998.

19. R.Z. Valiev and T.G. Langdon, *Acta Metall.*, **41**: p. 949, 1993.

20. Nieh, T.G. and J. Wadsworth, "Superplasticity and Superplastic Forming of Ceramics," *Materials Science Forum*, Vols. 170-172, pp. 259-268, 1994.

21. Nieh, T.G. and J. Wadsworth, "Superplastic behavior of a fine-grained, yttira stabilized tetragonal zirconia polycrystal (Y-TZP)," *Acta. Metall.*, **38**: pp.1121-1133, 1990.

22. C. Carry: in Ref. 2, p. 149.

23. Raj, R and C.K. Chyung, "Solution-Precipitation Creep in Glass Ceramics," *Acta Metall.*, **23**: pp. 159-166, 1986.

24. Clarke, D.R., "On the equilibrium thickness of intergranular glass phases in ceramic materials," *J. Am. Ceram. Soc.*, **70**: pp.15-22, 1987.

25. Schissler, D.J. A.H. Chokshi, T.G. Nieh and J. Wadsworth, "Microstructural Aspects of Superplastic Tensile Deformation and Cavitation Failure In a Fine-Grained Yttria Stabilized Tetragonal Zirconia," *Acta Metall. Mater.*, **39**: pp.3227-3236, 1991.

26. Klar, Erhard, ed., *Metals Handbook*. American Society for Metals, 1984.

27. Streeter, V.L. and E.B. Wylie, *Fluid Mechanics*, McGraw-Hill Publishing, Inc., 1985.

28. Rockett, T.J. and W.R. Foster, *J. Am. Ceram Soc.*, **48**: p. 78, 1965.

INITIAL DISTRIBUTION LIST

1. Defense Technical Information Center
   8725 John J. Kingman Rd., STE 0944
   Ft. Belvoir, VA 22060-6218 2

2. Dudley Knox Library
   Naval Postgraduate School
   411 Dyer Rd.
   Monterey, CA 93943-5101 2

3. Professor I. Dutta, Code ME/Du
   Department of Mechanical Engineering
   Naval Postgraduate School
   Monterey, CA 93943 2

4. Professor A. Gopinath, Code ME/Gk
   Department of Mechanical Engineering
   Naval Postgraduate School
   Monterey, CA 93943 2

5. Naval/Mechanical Engineering Curricular Office (Code 34)
   Department of Mechanical Engineering
   Naval Postgraduate School
   Monterey, CA 93943 1

6. LT Jason M. Lloyd
   4662 Gravelly Hills Road
   Louisville, TN 37777 5

7. LT Red Roeder
   Department of Mechanical Engineering
   Naval Postgraduate School
   Monterey, CA 93943 1